Journal of Rare Earths 42 (2024) 1–15

Contents lists available at ScienceDirect

Journal of Rare Earths

journal homepage: http://www.journals.elsevier.com/journal-of-rare-earths

Synthesis and applications of lanthanoid complexes of pentadentate and hexadentate N_5 and N_6 macrocycles: A review

Julio Corredoira-Vázquez [a, b], Cristina González-Barreira [a], Paula Oreiro-Martínez [a], Ana M. García-Deibe [a], Jesús Sanmartín-Matalobos [a, c], Matilde Fondo [a, *]

[a] Departamento de Química Inorgánica, Facultade de Química, Universidade de Santiago de Compostela, Campus Vida, 15782, Santiago de Compostela, Spain
[b] Phantom-g, CICECO – Aveiro Institute of Materials, Department of Physics, University of Aveiro, 3810-193, Aveiro, Portugal
[c] Institute of Materials (iMATUS), Universidade de Santiago de Compostela, 15782, Santiago de Compostela, Spain

ARTICLE INFO

Article history:
Received 31 October 2022
Received in revised form
6 March 2023
Accepted 16 March 2023
Available online 24 March 2023

Keywords:
Lanthanoid
N_5, N_6 macrocycle
Coordination chemistry
Chirality
Biological activity
Molecule magnet

ABSTRACT

In this paper, the lanthanoid complexes of N_5 and N_6 macrocycle ligands, without pendant arms or additional heteroatoms, are surveyed. This review covers the period from 2015 to the current date, since in 2014 Schiff base macrocyclic ligands incorporating the pyridine moiety, and their complexes, were revised, and in 2015 the chemistry of pentaaza macrocycle ligands with rare earth metals was also summarized. Porphyrin and phthalocyanine ligands are not included in this review, which primarily focuses on complexes with Schiff bases and amines without pendant arms or any additional donor other than nitrogen. The synthetic methods, structural characterization, based on single X-ray crystal data, and properties of the lanthanoid complexes, with special attention to magneto-structural correlations, are presented herein.

1. Introduction

The distinctive physical properties of the lanthanoid ions (Ln^{3+}) are crucial for their use in many areas of technology. Thus, the coordination chemistry of the lanthanoid metals is of interest in a variety of fields,[1] such as the search for new molecular magnetic materials,[2] catalysts,[3] luminescent thermometers,[4] or MRI contrast agents.[5] This is because the association of the Ln^{III} ion with adequate organic ligands induces a specific ligand field that can tailor and optimize the physico-chemical properties of the ion itself.

The design of N_5 and N_6 macrocyclic donors, and their related lanthanoid complexes, has been previously discussed and reviewed in a series of articles, published in the recent literature.[6,7] Nevertheless, remarkable efforts are currently aimed at the preparation, characterization, and application of lanthanoid complexes with this kind of donor, which is able to break the high selectivity of Ln^{III} ions towards hard Pearson bases, i.e., oxygen donors, and increase their affinity for nitrogen donors, all based on the additional stability of the macrocycle effect. These efforts are related to the alteration that the ligand can exert on the geometry and electronic features of the lanthanoid ions, which will result in a modulation of their physico-chemical characteristics. This modulation is clearly seen in single-molecule magnets (SMMs),[2,8] where the electrostatic field around the lanthanoid magnetic ion is a key point in allowing its efficient magnetic slow relaxation.

Tb^{III} and Dy^{III} are the Ln^{III} ions with the highest magnetic anisotropy, and this, joined to their high spin values ($S = 3$ for Tb^{III} and $S = 5/2$ for Dy^{III}) is the reason why they are the most used lanthanoid ions to build 4f-SMMs.[2,8,9] These oblate ions maximize their anisotropy with an axial geometry,[10] and, in fact, the best molecule magnet materials are organometallic Dy^{III} complexes with pseudolinear geometries.[11,12] But these compounds are unstable in air, and the coordination chemistry of lanthanoids with ligands that can help to promote air stable complexes with other highly axial geometries, such as pentagonal or hexagonal bipyramidal (PBP or HPB), is a promising area in the search for improved SMMs. In this way, the use of macrocyclic donors that can predetermine a weak equatorial N_5 or N_6 donor plane, is a good starting

* Corresponding author.
E-mail address: matilde.fondo@usc.es (M. Fondo).

https://doi.org/10.1016/j.jre.2023.03.013

point to introduce auxiliary hard donor ligands (O, F) in the apical positions, and thus obtain complexes of the oblate ions with strongly axial PBP or HPB geometries.

The use of macrocyclic ligands is important in determining not only the geometry, but also the stability, both in solid state and in solution. In this way, the relevant potential medical applications of lanthanoids, such as their use as MRI contrast agents or ratiometric optical thermometers, are highly dependent on their stability in aqueous solution.[4,5] Accordingly, older macrocyclic ligands are constantly being revisited, while new ones are being designed, in the search for lanthanoid compounds with various properties, and improved stabilities.

However, a recurring problem with the coordination chemistry of lanthanoids with pentaaza and hexaaza macrocycles is the difficulty in obtaining single crystals of the compounds, and knowing their exact structure. In fact, the vast majority of such compounds whose crystal structure is deposited in the CSD,[13] contain auxiliary nitrate ligands coordinated to the metal, in such a way that PBP or HPB geometries cannot be achieved. And the geometry has an enormous impact in many of the lanthanoid complexes properties, especially in magnetic and luminescent ones, and also in their catalytic or contrast agent abilities. For this reason, this work reviews the recent coordination chemistry of lanthanoids with N_5 and N_6 macrocycles without pendant arms, with special attention to their crystal structure and crystallization methods, as well as their applications in various fields. Since reviews on coordination chemistry of lanthanoid with macrocycles incorporating the pyridine fragment, and with pentaaza Schiff base macrocycles were published in 2014 and 2015,[6,7] respectively, the present revision of lanthanoid chemistry with N_5 and N_6 macrocycles will be limited from 2015 to the present. An additional review of molecule magnets that includes belt N_5 and N_6 macrocycles has also been published in 2022.[14] However, since this last revision focuses only on certain aspects of their magnetic properties, the methods of synthesis of these compounds, and a strong study of magneto-structural parameters which are not addressed in the aforementioned article, are also included.

2. Synthesis and crystallization

The complexes summarized herein are mostly derived from N_6 macrocycles, with very few compounds containing N_5 macrocycles. Irrespective of the number of ligand-donating nitrogen atoms, the complexes can be divided into two groups according to the type of ligand: a) Schiff bases or b) amines. Thus, the synthetic procedures depend on the kind of ligand.

2.1. Schiff base complexes

The macrocyclic Schiff base ligands (Scheme 1) with an N_6 (L^1-L^{11}),[15–29] or an N_5 (L^{12}-L^{14})[30–33] donor set are invariably derived from 2,6-pyridinedicarboxaldehyde[15–26,29] or 2,6-diacetylpyridine,[27,28,30–33] and various amines, with only one exception (L^{11}).[23] The vast majority of compounds with these ligands are mononuclear (Table 1), although some dinuclear compounds have also been published (Table 2).

2.1.1. Mononuclear complexes

Most of the mononuclear compounds (Table 1) were synthesized by a template method. Accordingly, 2,6-pyridindicarboxaldehyde or 2,6-diacetylpyridine, the corresponding amine and a lanthanoid salt were mixed in 2:2:1 or 1:1:1 molar ratios (Scheme 2).

Almost all the syntheses were performed under aerobic conditions, most of them in non-dry methanol as solvent (Table 1).[16,17,20–28,30–32] Nevertheless, in some cases, dry

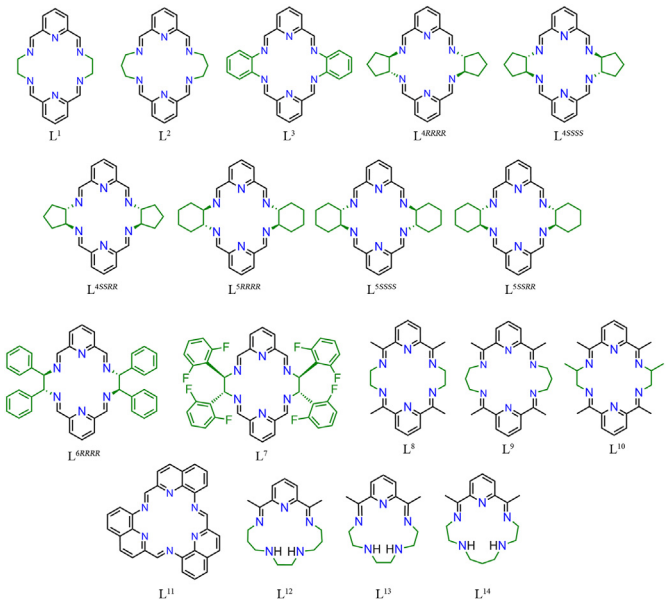

Scheme 1. N_5 and N_6 schiff base macrocycles.

methanol,[19] ethanol[15] or ethanol/acetonitrile[18] were used. The utilization of dried solvents seems more reasonable, given that in the formation of the Schiff base, water is obtained as a secondary product (Scheme 3), and the presence of additional water in the medium could lead to lower yields, and/or the formation of carbinolamines[34] or other hydrolyzed species,[35] which could result in isolation of impure products.

Some mononuclear complexes were obtained from other mononuclear precursors, by displacement of chloride[22,23,25,26,30,32] or acetate[27] donors by monoanionic oxygen ligands, as exemplified for a dysprosium acetate-complex precursor in Scheme 4. Thus, complexes of N_6 donors with R-triphenylsilanolate (R = H, 3-Br or 4-Br),[22,23,25–27] phenolate,[25] R-PhO$^-$ (R = 4-MeO,[25] 2,3,4,5,6-F,[25] 2,4-di-^{t}Bu[27]) or naphtholate,[25] as auxiliary ligands could be obtained by reacting the corresponding acetate or chloride mononuclear precursor with the oxygen donor in THF or CH_2Cl_2. The same method was used to isolate triphenylsilanolate,[30,32] binolate[22] or 2,6-Cl,4-NO_2-phenolate[32] dysprosium complexes of N_5 Schiff bases (Table 1), with the exception of the utilization of N_2 atmosphere in the isolation of some of the L^{14} complexes.[32] Besides, sometimes the intermediate chloride complexes were isolated,[25] while in other synthesis the reaction takes place without identifying these intermediates.[22,23,25,26,32]

Single crystals of the complexes were commonly obtained by slow evaporation of the liquor from the reaction (see Table S1).[15,18,23–25] In some cases, this evaporation took up to 5 weeks.[15] In other cases, the samples were recrystallized in water,[16] methanol[16] or mixtures of methanol and acetonitrile.[20,21] Some other complexes were crystallized by slow diffusion of diethyl ether in their dimethylformamide,[19] methanol,[25] chloroform[27] or dichloromethane[27] solutions, at room temperature,[19,25,27] or in the fridge, at *ca.* 5 °C.[27] Another alternative is layering saturated THF[25] or dichloromethane[30,32] solutions of the complex with hexane at room temperature[25,30,32] or in the freezer at −35 °C.[25] In some cases, the hexane layer on the dichloromethane solution was replaced by a layer of n-pentane.[22,23,26] Layering of the mother liquor with ethyl acetate at 4–6 °C has also been described, and in this case the crystallization process was delayed up to 5 months.[28]

Table 1
Mononuclear lanthanoid complexes derived from N_5 and N_6 macrocycle Schiff bases crystallographically characterized from 2015 to date.

Metal complex[a]	Reaction solvent	c.n./geom. [b]	Ref.
$[LnL^1(NCS)_3]$; Ln = Dy, Er	Dry EtOH	9/MFF	15
$[LnL^2(NCS)_3]$; Ln = Dy, Er	Dry EtOH	9/MFF	15
$[LnL^3(NCS)_3]$; Ln = Dy, Er	Dry EtOH	9/HH	15
$[LnL^1(NO_3)_3]$; Ln = Ce, Pr	MeOH	12/IC	16
$[EuL^1(NO_3)(H_2O)_2](NO_3)_2$	MeOH	10/TD	16
$[TbL^1(NO_3)_2](NO_3)$	MeOH	10/TD	17
$[TbL^1(NCS)_3]$	Dry EtOH/MeCN	9/MFF	18
$[TbL^2(NCS)_3]$	Dry EtOH/MeCN	9/MFF	18
$[TbL^3(NCS)_3]$	Dry EtOH/MeCN	9/MFF	18
$[LnL^3(NO_3)_3]$; Ln = La, Ce	Dry MeOH	12/IC	19
$[Nd(L^{4RRRR})Cl(H_2O)_2]Cl_2$	MeOH	9/HH	20
$\{[Nd(L^{4RRRR})Cl(H_2O)_2]Cl_2\}$	MeOH	9/HH	20
$\{[Nd(L^{4SSSS})Cl(H_2O)_2]Cl_2\}$			
$[Nd(L^{4SSRR})Cl(H_2O)_2]Cl_2$	MeOH	9/HH	20
$[Yb(L^{4RRRR})(NO_3)_2](NO_3)$	MeOH	10/TD	21
$[Dy(L^{5RRRR})(Ph_3SiO)_2](BPh_4)$	$MeOH/CH_2Cl_2/H_2O$	8/HBP	22
$[Dy(L^{5SSSS})(Ph_3SiO)_2](BPh_4)$	$MeOH/CH_2Cl_2/H_2O$	8/HBP	22
$[Dy(L^{5RRRR})(Ph_3SiO)_2][(3\text{-}Br\text{-}Ph)BPh_3]$	$MeOH/CH_2Cl_2/H_2O$	8/HBP	23
$[Dy(L^{5SSSS})(Ph_3SiO)_2][(3\text{-}Br\text{-}Ph)BPh_3]$	$MeOH/CH_2Cl_2/H_2O$	8/HBP	23
$[Dy(L^{5RRRR})(Ph_3SiO)_2][(4\text{-}Br\text{-}Ph)BPh_3]$	$MeOH/CH_2Cl_2/H_2O$	8/HBP	23
$[Dy(L^{5SSSS})(Ph_3SiO)_2][(4\text{-}Br\text{-}Ph)BPh_3]$	$MeOH/CH_2Cl_2/H_2O$	8/HBP	23
$[La(L^{6RRRR})Cl_3]$	MeOH	9/HH	24
$\{[Tb(L^{6RRRR})Cl_2(MeOH)]$	MeOH	9/HH	24
$[Tb(L^{6RRRR})Cl_2(H_2O)]\}Cl_2$			
$[DyL^6Cl_2(H_2O/CH_3OH)]Cl$	MeOH	9/HH	25
$[DyL^6(C_6F_5O)_2(H_2O)](BPh_4)$	THF	9/HH	25
$[DyL^6(PhO)_2](BPh_4)$	THF	8/HBP	25
$[DyL^6(4\text{-}MeO\text{-}PhO)_2](BPh_4)$	THF	8/HBP	25
$[DyL^6(naphtolate)_2](BPh_4)$	THF	8/HBP	25
$[DyL^6(Ph_3SiO)_2](BPh_4)$	THF	8/HBP	25
$[DyL^{7RRRR}(Ph_3SiO)_2](PF_6)$	$MeOH/CH_2Cl_2/H_2O$	8/HBP	26
$[DyL^{7SSSS}(Ph_3SiO)_2](PF_6)$	$MeOH/CH_2Cl_2/H_2O$	8/HBP	26
$[DyL^{7RRRR}(4Br\text{-}Ph_3SiO)_2](PF_6)$	$MeOH/CH_2Cl_2/H_2O$	8/HBP	26
$[DyL^{7SSSS}(4Br\text{-}Ph_3SiO)_2](PF_6)$	$MeOH/CH_2Cl_2/H_2O$	8/HBP	26
$[DyL^8(CH_3CO_2)_2](CH_3CO_2)$	MeOH	10/TD	27
$[DyL^8(2,4\text{-}di\text{-}^tBu\text{-}PhO)_2](BPh_4)$	CH_2Cl_2	8/HBP	27
$[DyL^8(Ph_3SiO)_2](BPh_4)$	CH_2Cl_2	8/HBP	27
$[DyL^8(Ph_3SiO)_2](PF_6)$	CH_2Cl_2	8/HBP	27
$[LaL^{10}(MeOH)(NO_3)_2](NO_3)$	MeOH	11/JCPAPR	28
$[DyL^{11}(Ph_3SiO)_2](ClO_4)$	MeCN	8/HBP	23
$[DyL^{11}(Ph_3SiO)_2](OTf)$	MeCN	8/HBP	23
$[DyL^{12}(Ph_3SiO)_2](BPh_4)$	$MeOH/CH_2Cl_2/H_2O$	7/PBP	30
$[DyL^{13}(Cl)_2](Cl)$	MeOH	7/PBP	31
$[DyL^{14}(BINOL^R)_2](BPh_4)$	$MeOH/CH_2Cl_2/H_2O$	7/PBP	22
$[DyL^{14}(BINOL^S)_2](BPh_4)$[b]	$MeOH/CH_2Cl_2/H_2O$	7/PBP	22
$[DyL^{14}(Ph_3SiO)_2](BPh_4)$	$MeOH/CH_2Cl_2/H_2O$	7/PBP	32
$[DyL^{14}(2,6\text{-}Cl\text{-}4\text{-}NO_2\text{-}PhO)_2](BPh_4)$	$MeOH/CH_3CN/THF$	7/PBP	32

[a] Solvates are omitted, ligands in Scheme 1.
[b] MFF: muffin, HH: hula-hoop, IC: icosahedron, TD: tetradecahedron, HBP: hexagonal bipyramid, JCPAPR: capped pentagonal antiprism, PBP: pentagonal bipyramid.

2.1.2. Dinuclear complexes

A smaller number of dinuclear compounds have been described (Table 2).[16,21,22,24,29,33] These are generally obtained from mononuclear precursors, by reacting them with a potential bridging ligand. Thus, $[Yb_2(L^{4SSSS})_2(\mu\text{-}OH)_2(H_2O)_2](NO_3)_4$ and $[Yb_2(L^{4RRRR})_2(\mu\text{-}OH)_2(H_2O)_2][Yb_2(L^{4SSSS})_2(\mu\text{-}OH)_2(H_2O)_2](NO_3)_8$ were isolated after stirring the pure enantiomeric $[Yb(L^{4RRRR})(NO_3)_2](NO_3)$ or racemic $[Yb(L^{4rac})(NO_3)_2](NO_3)$ precursors with a solution of sodium hydroxide in methanol/water.[21] Basically, the same synthetic procedure was used in the isolation of $[Nd_2(L^{5SSSS})_2(\mu\text{-}OH)_2(NO_3)_2](NO_3)_2$, $[Eu_2(L^{5RRRR})_2(\mu\text{-}OH)_2(NO_3)_2](NO_3)_2$ or $\{[Yb_2(L^{5SSSS})_2(\mu\text{-}OH)_2(H_2O)_2][Na(NO_3)_3(H_2O)_2](NO_3)_2\}$,[29] just varying the solvent of the reaction. However, the hydroxide bridged complexes $[Dy_2(L^{5RRRR})_2(\mu\text{-}OH)_2(4\text{-}MeSPhO)_2](BPh_4)$ or $[Dy_2(L^{5SSSS})_2(\mu\text{-}OH)_2(4\text{-}MeSPhO)_2](BPh_4)$ were isolated in one pot template synthesis, by mixing $DyCl_3{\cdot}6H_2O$, 2,6-diformylpyridine, diaminocyclohexane, 4-MeSPhOH, Et_3N and $NaBPh_4$.[22]

Dinuclear fluoride bridged $[La_2(L^{6RRRR})_2(\mu_2\text{-}F)_3F(H_2O)]Cl_2$, $[Yb_2(L^{5RRRR})_2(\mu_2\text{-}F)_2F(H_2O)]Cl_3$ or $[Lu_2(L^{5RRRR})_2(\mu_2\text{-}F)_2(NO_3)_2](NO_3)_2$ complexes have also been obtained from the corresponding monomeric chloride or nitrate precursor, by addition of a stoichiometric amount of potassium or tetraethylamonium fluoride.[24] Nevertheless, the polymer complex $[Dy_2(L^{14})_2\{Fe(CN)_6\}(\mu\text{-}CO_3)(OH)]_n$, made up of dinuclear $[Dy_2(L^{14})_2(\mu\text{-}CO_3)(OH)]^{3+}$ moieties joined through $[Fe(CN)_6]^{3-}$ linkers (Fig. 1), was prepared by a template method, from $DyCl_3{\cdot}6H_2O$, 2,6-diacetylpyridine, 3,7-diazanonane-1,9-diamine and $K_3[Fe(CN)_6]$ in methanol/water.[33]

Single crystals of all the dinuclear hydroxide-bridged complexes were grown by slow evaporation of their methanol or water solutions,[21,29] or by layering a dichloromethane solution of the complex with n-pentane at room temperature for several days.[22] Single crystals of the fluoride bridged compounds were prepared *in situ* from evaporation of methanol or chloroform/methanol solutions containing mixtures of $[La(L^{6RRRR})(Cl)_3]$, $[Yb(L^{5RRRR})(Cl)_3]$ or $[Lu(L^{5RRRR})(NO_3)_2](NO_3)$, and NEt_4F or KF in different mononuclear complex:fluoride molar ratio (1:1, 1:1.5 or 1:2).[24] Crystals of the polymer compound $[Dy_2(L^{14})_2\{Fe(CN)_6\}(\mu\text{-}CO_3)(OH)]_n$ (Fig. 1) were isolated from a sealed tube containing the mother liquor of the reaction after one month.[33]

2.2. Amine complexes

A scarce number of lanthanoid compounds crystallographically characterized with the amine ligands L^{15}-L^{16}, and the amine-imine ligand L^{17} (Scheme 5), have been reported since 2015 (Table 3).[36–38] The L^{15}-L^{16} N_6 amines were typically isolated as free ligands from a template reaction between the corresponding aldehyde and amine, in the presence of a metal salt, followed by reduction of the formed Schiff base with $NaBH_4$, and subsequent work-up (Scheme 6).[39,40]

The asymmetric amine-imine L^{17} was not isolated as a free ligand.[38] The obtention of complexes of L^{17} is a complicated process (Scheme 7),[38] where the key element is the protection of one of the formyl groups of the dialdehyde via acetalization with ethylene glycol. Subsequent treatment with the corresponding isomer of diaminocyclohexane, reduction with $NaBH_4$, deprotection of the groups, and reaction with ethylenediamine in the presence of the lanthanoid salt, finally yields $[LnL^{17}(NO_3)_2](NO_3)$ (Ln = Eu, Yb) compounds.

The mononuclear complexes derived from L^{15} and L^{16} were prepared in a classical synthesis from the ligands and metal salts, in water[36] or acetonitrile[37] at high temperature (reflux). The only dinuclear complex $[Eu_2L^{15}(\mu_2\text{-}CO_3)(H_2O)_3]Cl_4$, where the diastereoisomeric macrocycle L^{15} is observed, was isolated from the precursor $[Eu(L^{15})Cl(H_2O)]Cl_2$, by reaction with sodium carbonate in water at room temperature.[36]

Single crystals of all the mononuclear amine or amine/imine complexes were obtained by slow evaporation of methanol,[36] acetonitrile[37] or mixed methanol/chloroform[38] solutions of the corresponding compounds. Single crystals of dinuclear complex $[Eu_2L^{15}(\mu_2\text{-}CO_3)(H_2O)_3]Cl_4$ were grown by slow evaporation of a water solution containing $[Eu(L^{15})Cl(H_2O)]Cl$ and K_2CO_3 in an inert atmosphere.[36]

3. Structural features

3.1. Schiff bases complexes

The crystal structures of the Schiff base complexes (Tables 1 and 2) show different structural features. Thus, the geometry around the metal centers of the mononuclear compounds seems to depend on the size of the metal ion, the lanthanoid salt employed, and the denticity of the macrocycle.

Table 2
Dinuclear or polynuclear lanthanoid complexes derived from N_5 and N_6 macrocycle Schiff bases crystallographically characterized from 2015 to date.

Metal complex[a]	Reaction solvent	c.n./geom.[b]	Ref.
$[La_2L^1(CO_3)_2(NO_3)_2(H_2O)]_n$	H_2O	9/HH 10/TD	16
$[Yb_2(L^{4SSSS})_2(\mu\text{-}OH)_2(H_2O)_2](NO_3)_4$	$MeOH/CHCl_3$	9/HH	21
$[Yb_2(L^{4RRRR})_2(\mu\text{-}OH)_2(H_2O)_2]$ $[Yb_2(L^{4SSSS})_2(\mu\text{-}OH)_2(H_2O)_2](NO_3)_8$	$MeOH/CHCl_3$	9/HH	21
$[Dy_2(L^{5RRRR})_2(\mu\text{-}OH)_2(4\text{-}MeSPhO)_2](BPh_4)$	$MeOH/CH_2Cl_2/H_2O$	9/HH	22
$[Dy_2(L^{5SSSS})_2(\mu\text{-}OH)_2(4\text{-}MeSPhO)_2](BPh_4)$	$MeOH/CH_2Cl_2/H_2O$	9/HH	22
$[Nd_2(L^{5SSSS})_2(\mu\text{-}OH)_2(NO_3)_2](NO_3)_2$	H_2O	10/TD	29
$[Eu_2(L^{5RRRR})_2(\mu\text{-}OH)_2(NO_3)(H_2O)](NO_3)_3$	MeOH	9/HH 10/TD	29
$\{[Yb_2(L^{5SSSS})_2(\mu\text{-}OH)_2(H_2O)_2][Na(NO_3)_3(H_2O)_2](NO_3)_2\}$	MeOH	9/HH	29
$[La_2(L^{6RRRR})_2(\mu_2\text{-}F)_3F(H_2O)]Cl_2$	MeOH	10/JSPC 10/JBCSAPR	24
$[Yb_2(L^{5RRRR})_2(\mu_2\text{-}F)_2F(H_2O)]Cl_3$	MeOH	9/MFF	24
$[Lu_2(L^{5RRRR})_2(\mu_2\text{-}F)_2(NO_3)_2](NO_3)_2$	MeOH	10/JSPC 10/TD	24
$[Dy_2(L^{14})_2\{Fe(CN)_6\}(\mu\text{-}CO_3)(OH)]_n$	$MeOH/H_2O$	8/TDD	33

[a] Solvates are omitted, ligands in Scheme 1.
[b] HH: hula-hoop, TD: tetradecahedron, JSPC: sphenocorona, JBCSAPR: bicapped square antiprism, MFF: muffin, TDD: triangular dodecahedron.

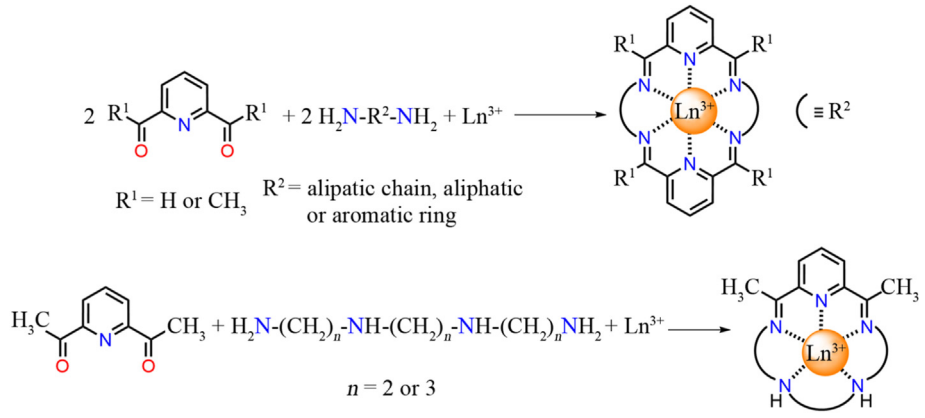

Scheme 2. Reactions for isolation of lanthanoid-Schiff base N_6 or N_5 macrocycles. Auxiliary donors are omitted for clarity.

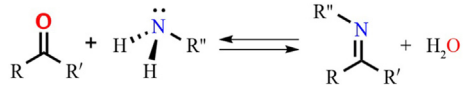

Scheme 3. Schematic representation of the reaction for isolation of imines.

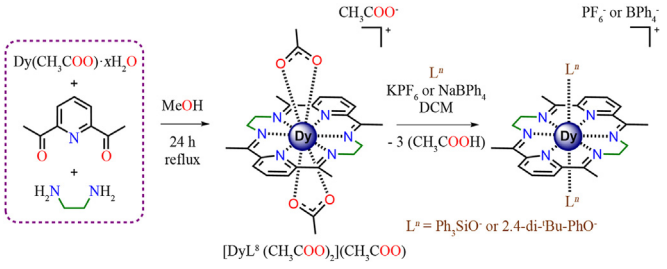

Scheme 4. Isolation of mononuclear dysprosium complexes with auxiliary monodentate oxygen-donors from a dysprosium acetate-complex precursor. Adapted with permission from Ref. 27. Copyright 2019 Wiley.

3.1.1. Mononuclear complexes

The coordination numbers for the mononuclear compounds (Table 1) vary from 12 to 7. Those with the highest coordination numbers are the ones with the larger lanthanoid ions, and quite small potentially bidentate auxiliary donors. Accordingly, only La^{III}, Ce^{III} and Pr^{III} can achieve coordination number (c.n.) 12 when they interact with an N_6 macrocycle and nitrate as an auxiliary ligand (see, for example, Fig. 2), yielding mononuclear $[LnL^X(NO_3)_3]$ ($X = 1$ or 3) compounds.[16,19] The N_6O_6 environment of the Ln^{III} ions leads to a geometry closer to an icosahedron (Table 1), in agreement with SHAPE[41] measurements. It is described a unique case of a lanthanum complex with an N_6 donor and nitrate as ligand, ($[LaL^{10}(MeOH)(NO_3)_2](NO_3)$, Fig. 3), with coordination number lower than 12 (11), and capped pentagonal antiprism geometry.[28]

However, when the lanthanoid ions are smaller, like Tb^{III}, Eu^{III} or Yb^{II}, complexes with nitrate ancillary donors can also be obtained, with empirical formulas $[LnL^X(NO_3)_2](NO_3)$ (Ln = Tb, $X = 1$; or Ln = Yb, $X = 4RRRR$)[17,21] or $[EuL^1(NO_3)(H_2O)_2](NO_3)_2$,[16] but all of them show coordination number 10, as exemplified in Fig. 4,[17] with a geometry closer to the tetradecahedron,[16,17,21] according to SHAPE calculations.[41] The same geometry is found in $[DyL^8(CH_3CO_2)_2](CH_3CO_2)$ (Scheme 4), which contain bidentate acetate donors[27] instead of the nitrate ones.

Nevertheless, when the auxiliary ligands are monodentate, the coordination numbers diminish. In this way, mononuclear complexes with ancillary chloride ligands do not exceed coordination number 9, independently of the size of the Ln^{III} ion (Ln = La, Nd, Tb or Dy).[20,24,25] Thus, most of these complexes with N_6 donors

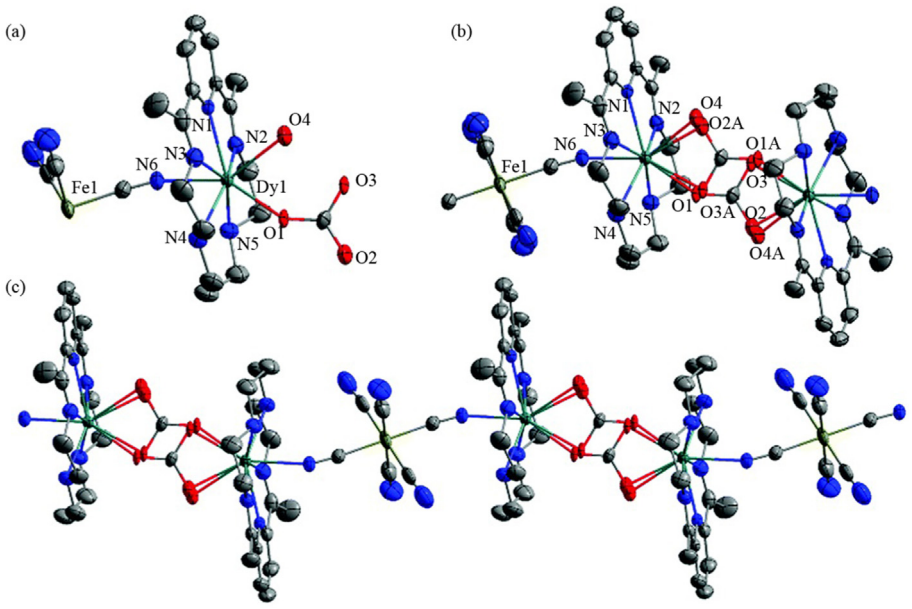

Fig. 1. (a, b) A structural unit for $[Dy_2(L^{14})_2\{Fe(CN)_6\}(\mu\text{-}CO_3)(OH)]_n$; (c) Portion of the 1-D chain for $[Dy_2(L^{14})_2\{Fe(CN)_6\}(\mu\text{-}CO_3)(OH)]_n$. Adapted with permission from Ref. 33. Copyright 2022 Royal Society of Chemistry.

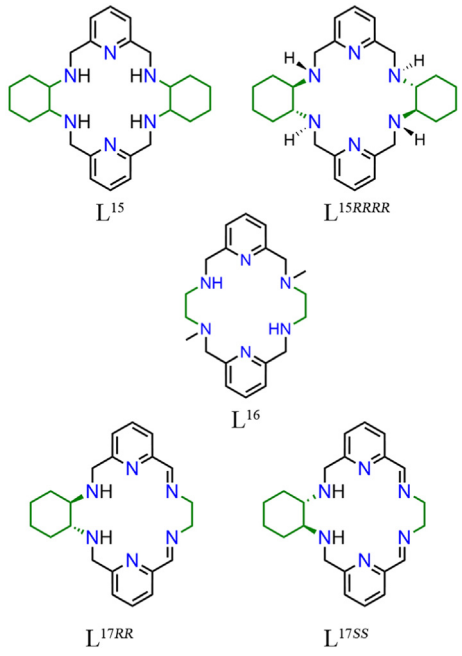

Scheme 5. Amine and amine/imine macrocycle N_5 and N_6 ligands.

present c.n. 9 with hula hoop geometry,[20,24,25] according to SHAPE calculations, as exemplified for $[LaL^{6RRRRR}Cl_3]$ in Fig. 5.[24] Moreover, the only described dysprosium compound with the N_5 macrocycle L^{13} and chloride ancillary ligands seems to show c.n. 7 with a PBP environment.[31]

All the published complexes with thiocyanate and N_6 macrocycles as ligands exhibit the empirical formula $[LnL^X(NCS)_3]$ (Ln = Tb, Dy, Er; X = 1, 2 or 3), with c.n. 9, and preferent muffin geometry,[15,18] as $[TbL^2(NCS)_3]$ (Fig. 6).[18]

The introduction of bulky auxiliary donors diminishes the coordination numbers, although sometimes the metal center binds more ligands than would be expected. Accordingly, the complex

Table 3
Lanthanoid complexes derived from N_6 macrocyclic amine or amine/imine ligands crystallographically characterized from 2015 to date.

Metal complex[a]	Reaction solvent	c.n./geom.[b]	Ref.
$[Dy(L^{15RRRR})Cl(H_2O)]Cl_2$	H_2O	8/TDD	36
$[Eu_2(L^{15})_2(\mu_2\text{-}CO_3)(H_2O)_3]Cl_4$	H_2O	9/MFF	36
$[CeL^{16}(NO_3)_2](NO_3)$	MeCN	10/TD	37
$[SmL^{16}(NO_3)_2](NO_3)$	MeCN	10/TD	37
$[YbL^{17SS}(NO_3)_2](NO_3)$	MeOH	10/JBCSAPR	38
$[EuL^{17RR}(NO_3)_2](NO_3)$	MeOH	10/TD	38

[a] Solvates are omitted, ligands in Scheme 5.
[b] TDD: triangular dodecahedron, MFF: muffin, TD: tetradecahedron, JBCSAPR: bicapped square antiprism.

$[DyL^6(C_6F_5O)_2(H_2O)](BPh_4)$,[25] which contains the quite bulky 2,3,4,5,6-pentafluorophenolate ligand, can link an additional water molecule to give rise to a nonacoordinate environment of the Dy^{III} ion, with hula hoop geometry (Fig. 7).[25]

Nevertheless, complexes with coordination number 8 and HBP geometry are obtained from N_6 macrocycles and R-PhO^- (R = H, 4-MeO or 2,4-di-^{t}Bu),[25,27] R-Ph_3SiO^- (R = H, 3-Br or 4-Br)[22,23,26,27] or naphthtolate[25] as ancillary donors, as exemplified in Fig. 8.[27] This kind of ligand effectively blocks the axial positions, and leads to coordination number 7 with PBP geometry when the macrocycle is a N_5 donor,[22,30,32] as in $[DyL^{12}(Ph_3SiO_2)_2](BPh_4)$ (Fig. 9).[30]

3.1.2. Di- or polinuclear complexes

All the dinuclear compounds described since 2015 derive from N_6 macrocycles, while the only polymer $[Dy_2(L^{14})_2\{Fe(CN)_6\}(\mu\text{-}CO_3)(OH)]_n$ (Fig. 1),[33] made up of dinuclear units, contains the pentadentate L^{14} ligand. In all these complexes, the metal centers do not exceed coordination number 10, independently of the metal ion employed. Nonetheless, once more, the size of the Ln^{III} ion, and the denticity of the auxiliary donors, seem to play a fundamental role. Accordingly, the highest coordination numbers are achieved for larger lanthanoid ions and/or potentially bidentate ancillary ligands.[16,24,29] However, the type of bridge (hydroxide, fluoride or carbonate) does not seem to have too much influence on the

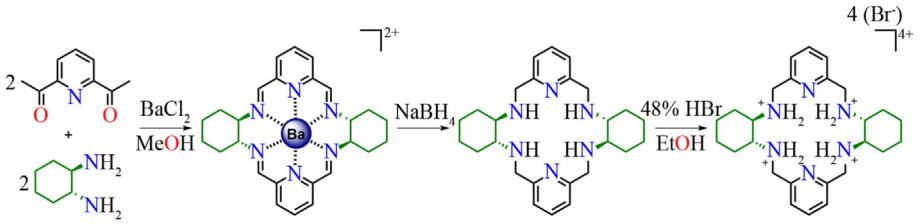

Scheme 6. Route for the isolation of L^{15}. Adapted with permission from Ref. 39. Copyright 1996 Elsevier.

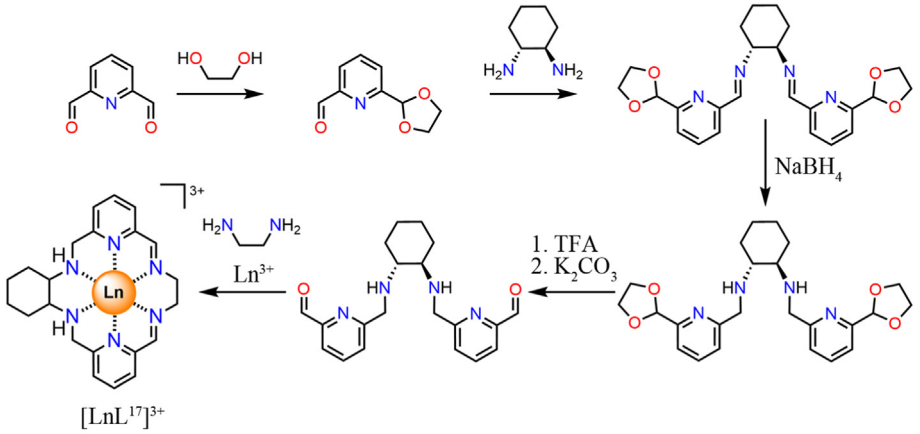

Scheme 7. Reaction scheme for the isolation of lanthanoid complexes derived of L^{17}. Auxiliary donors and/or counterions are omitted for clarity. Adapted with permission from Ref. 38. Copyright 2021 Elsevier.

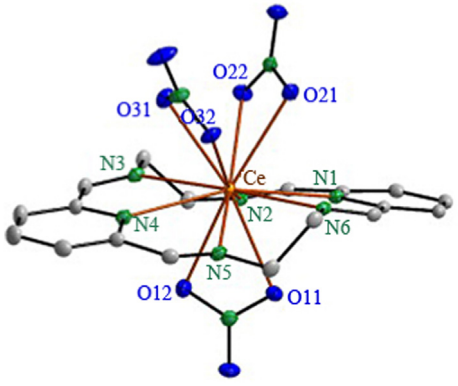

Fig. 2. Crystal structure of $[CeL^{1}(NO_3)_3]$. Reproduced with permission from Ref. 16. Copyright 2015 Elsevier.

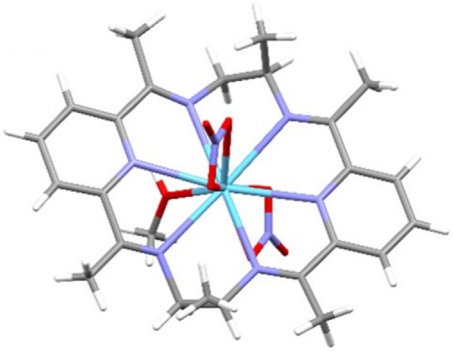

Fig. 3. Sticks representation of the crystal structure of $[LaL^{10}(MeOH)(NO_3)_2]^+$ in $[LaL^{10}(MeOH)(NO_3)_2](NO_3)$. Color code: light blue: lanthanum; light mauve: nitrogen; red: oxygen; grey: carbon; white: hydrogen. Reproduced with permission from Ref. 28. Copyright 2021 American Chemical Society.

coordination number achieved by the metal center. In this way, coordination number 10 is only attained by the large La^{III},[16] Nd^{III} and Eu^{III} ions,[29] and by the small Lu^{III},[24] when nitrate ions act as bidentate ligands, as exemplified in Fig. 10.[29]

Besides, the large La^{III} also achieves coordination number 10 in the presence of monodentate fluoride and water donors (Fig. 11).[24] Once again, the preferred geometry for this c.n. is the tetradodecahedron, although in $[La_2(L^{6RRRR})_2(\mu_2\text{-}F)_3F(H_2O)]Cl_2$ the environment of the ions is distorted capped pentagonal antiprism or bicapped square antiprism.

All the ytterbium complexes with N_6 macrocycles, and additional monodentate water or fluoride donors, are nonacoordinate, independently of the μ-OH[21] or μ-F bridge,[22] as exemplified by $[Yb_2(L^{5RRRR})_2(\mu_2\text{-}F)_2F(H_2O)]Cl_3$ in Fig. 12.[24] But, although the type of bridge does not seem to alter the coordination number, it seems to

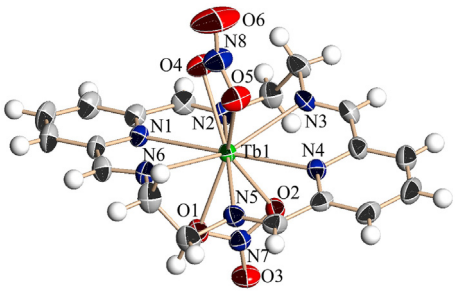

Fig. 4. Ellipsoids diagram for $[TbL^{1}(NO_3)_2]^+$ in $[TbL^{1}(NO_3)_2](NO_3)$. Reproduced with permission from Ref. 17. Copyright 2021 Elsevier.

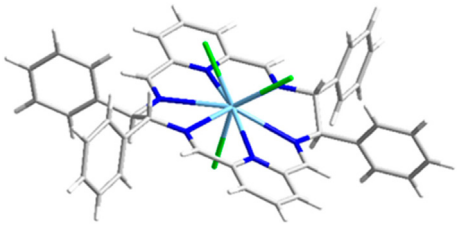

Fig. 5. Sticks representation of the crystal structure of $[LaL^{6RRRR}Cl_3]$. Color code: light blue: lanthanum; deep blue: nitrogen; green: chloride; grey: carbon; white: hydrogen. Reproduced with permission from Ref. 24. Copyright 2021 American Chemical Society.

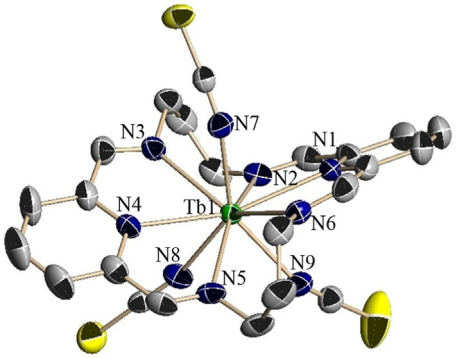

Fig. 6. Ellipsoids diagram for $[TbL^2(NCS)_3]$. Reproduced with permission from Ref. 18. Copyright 2021 Wiley.

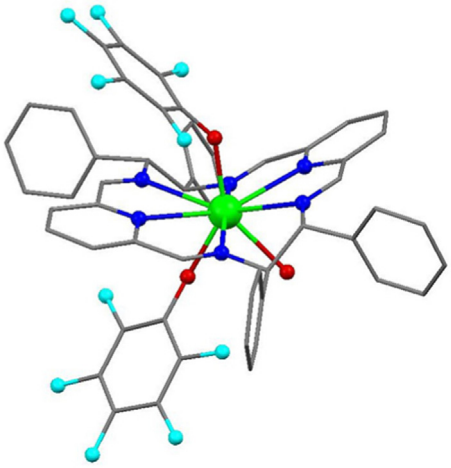

Fig. 7. Balls and sticks diagram for $[DyL^6(C_6F_5O)_2(H_2O)]^+$ in $[DyL^6(C_6F_5O)_2(H_2O)](BPh_4)$. Color codes: green: dysprosium; deep blue: nitrogen; red: oxygen; light blue: fluoride; grey: carbon; hydrogens are omitted. Reproduced with permission from Ref. 25. Copyright 2019 Wiley.

have a great impact on the geometry, given that the hydroxide bridged complexes present a hula-hoop geometry,[21,22,29] while the only complex with the fluoride bridge that meets the mentioned requirements shows the Yb^{III} center in a muffin environment,[24] according to SHAPE measurements.[41,42]

The only polymer $[Dy_2(L^{14})_2\{Fe(CN)_6\}(\mu\text{-}CO_3)(OH)]_n$, which contains the N_5 macrocycle L^{14}, presents octacoordinated dysprosium centers in triangular dodecahedral environments (Fig. 1).[33]

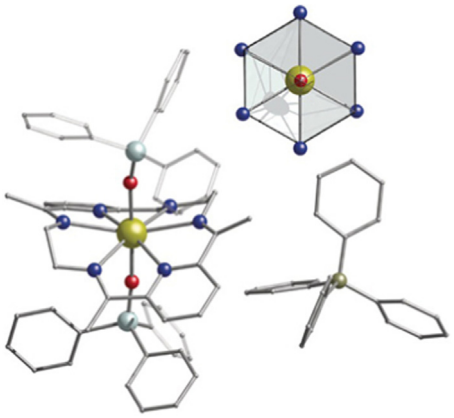

Fig. 8. Balls and sticks diagram for $[DyL^8(Ph_3SiO_2)_2](BPh_4)$. Color codes: gold: dysprosium; blue: nitrogen: red: oxygen; light turquoise:silicon; gray: carbon; dark yellow: boron. Hydrogen atoms are omitted. Reproduced with permission from Ref. 27. Copyright 2019 Wiley.

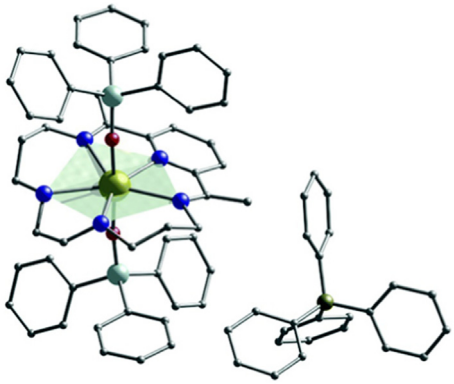

Fig. 9. Balls and sticks diagram for $[DyL^{12}(Ph_3SiO_2)_2](BPh_4)$. Color codes: gold: dysprosium; blue: nitrogen: red: oxygen; light turquoise: silicon; gray: carbon; dark yellow: boron. Hydrogen atoms are omitted. Reproduced with permission from Ref. 30. Copyright 2020 Royal Society of Chemistry.

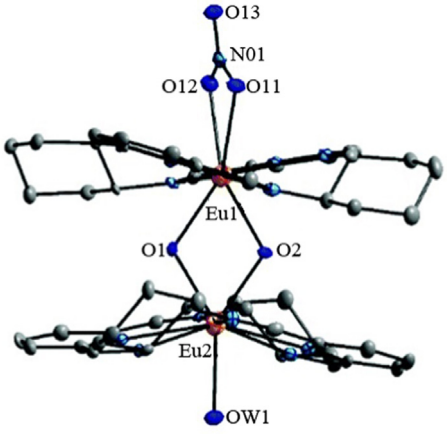

Fig. 10. Balls and sticks diagram for the cation $[Eu_2(L^{5RRRR})_2(\mu\text{-}OH)_2(NO_3)(H_2O)]^{3+}$ in $[Eu_2(L^{5RRRR})_2(\mu\text{-}OH)_2(NO_3)(H_2O)](NO_3)_3$, showing c.n. number 10 for Eu1, with nitrate coordinated as a bidentate ligand, and c.n. number 9 for Eu2, where all the auxiliary ligands are monodentate. Color codes: orange: europium; light blue: nitrogen: deep blue: oxygen; gray: carbon. H-atoms are omitted. Reproduced with permission from Ref. 29. Copyright 2019 Royal Society of Chemistry.

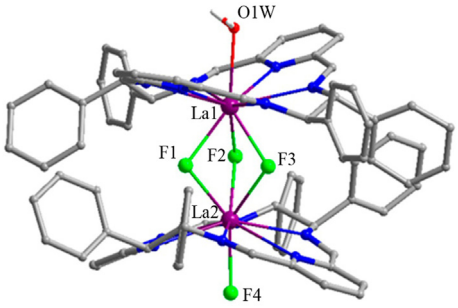

Fig. 11. Balls and sticks representation for of the crystal structure of $[La_2(L^{6RRRR})_2(\mu_2\text{-}F)_3F(H_2O)]^{2+}$ in $[La_2(L^{6RRRR})_2(\mu_2\text{-}F)_3F(H_2O)]Cl_2$. Reproduced with permission from Ref. 24. Copyright 2021 American Chemical Society.

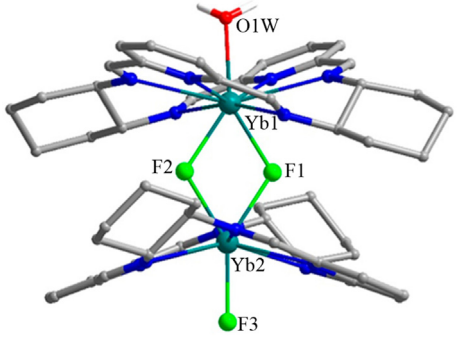

Fig. 12. Balls and sticks representation of the crystal structure of $[Yb_2(L^{5RRRR})_2(\mu_2\text{-}F)_2F(H_2O)]^{3+}$ in $[Yb_2(L^{5RRRR})_2(\mu_2\text{-}F)_2F(H_2O)]Cl_3$. Reproduced with permission from Ref. 24. Copyright 2021 American Chemical Society.

As a summary, it can be said that the large Ln^{III} ions with ancillary potentially bidentate donors lead to the highest coordination numbers, which do not exceed number 12. These highest coordination numbers are attained in mononuclear complexes, given that c.n. 10 is not exceeded in di- or polynuclear compounds. Besides, the most common coordination numbers, independently of the nuclearity of the complex, are 9 and 10, with preferent hula-hoop and tetradodecahedral geometries, respectively. In addition, the presence of bulky monodentate auxiliary donors, effectively blocks the axial positions and predetermine HBP (with N_6 macrocycles) or PBP (with N_5 macrocycles) geometries in mononuclear coordination compounds.

3.2. Amine complexes

The vast majority of the complexes derived from the amine N_6 macrocycles L^{15} and L^{16}, and from amine/imine N_6 donor L^{17} are mononuclear compounds (Table 3).[36–38] In fact, just $[Eu_2L^{15}(\mu_2\text{-}CO_3)(H_2O)_3]Cl_4$ is a dinuclear species.[36] As in the Schiff base complexes, the coordination number depends not only on the size of the lanthanoid ion, but in the denticity of the ancillary donors. Accordingly, complexes $[LnL^X(NO_3)_2](NO_3)$ (X = 16, Ln = Ce, Sm; X = 17*SS*, Ln = Yb; X = 17*RR*, Ln = Eu) present coordination number 10, with preferred tetradodecahedral geometry (Fig. 13),[37,38] except for the Yb^{III} compound, which is a bicapped square antiprism.[38] Thus, it seems that the compounds with amine donors diminish the coordination numbers with respect to those with the more rigid Schiff bases ligands (c.n. 12 for $[CeL^X(NO_3)_3]$, with X = 1, 3).

The only mononuclear amine complex with monodentate auxiliary ligands, $[Dy(L^{15RRRR})Cl(H_2O)]Cl_2$, is the one with the lowest coordination number among amine and mixed amine/imine

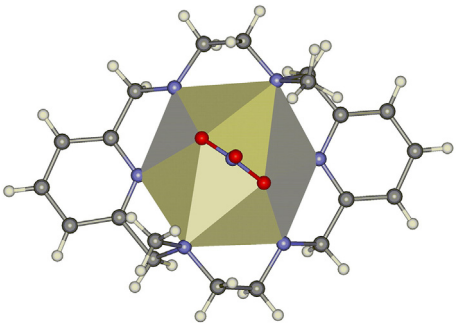

Fig. 13. Balls and sticks representation of the crystal structure of $[CeL^{16}(NO_3)_2]^{3+}$ in $[CeL^{16}(NO_3)_2](NO_3)$, showing the TDD environment of the cerium atom. Reproduced with permission from Ref. 37. Copyright 2019 Elsevier.

compounds. In this case, the c.n is 8, with triangular dodecahedral geometry (Fig. 14).[36] It is noticeable that this is the only triangular dodecahedral complex of an N_6 macrocycle with c.n. 8, provided that the other reported complexes of this kind are HBP, and this shows the effect of the flexibility of the ligand in the geometry of the complex. Hence, it seems that the flexible amine N_6 macrocycles cannot predetermine the HBP geometry.

The unique dinuclear complex $[Eu_2(L^{15})_2(\mu_2\text{-}CO_3)(H_2O)_3]Cl_4$, which contains the larger Eu^{III} and terminal monodentate ligands, in addition to the μ_2-CO_3 bridge, presents coordination number 9 (which is higher than in the $[Dy(L^{15RRRR})Cl(H_2O)]Cl_2$ (8) complex with the smaller Dy^{III} ion), and a muffin structure (Fig. 15).[36]

4. Properties

The complexes summarized herein present different properties that improve their interest and potential applications. The most relevant ones, which include chirality, biological activity, and molecule magnet behavior, are discussed below. Some aspects of the magnetic properties of the mononuclear PBP and HBP complexes were recently reviewed.[14] Therefore, in this revision, in addition to incorporating some new compounds, the emphasis is placed on magneto-structural correlations of Dy^{III} single ion magnets (SIMs) that were not previously analyzed. Besides, it is also worth mentioning that complexes $[LnL^3(NO_3)_3]$ (Ln = La, Ce) show the interesting property of acting as n-dopants of graphene for achieving air stable graphene field-effect-transistors, with symmetric transconductance, and high operational current densities.[19]

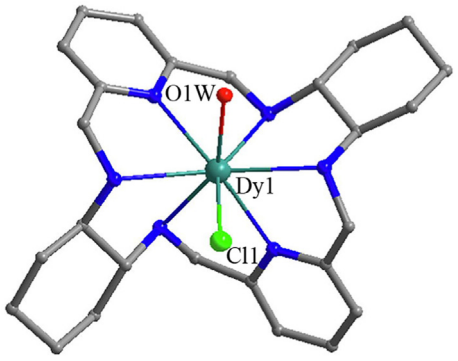

Fig. 14. Balls and sticks representation of the crystal structure of $[Dy(L^{15RRRR})Cl(H_2O)]^{2+}$ in $[Dy(L^{15RRRR})Cl(H_2O)]Cl_2$. Color codes: blue-green: dysprosium; blue: nitrogen; red: oxygen; gray: carbon. Hydrogen atoms are omitted. Reproduced with permission from Ref. 36. Copyright 2019 Elsevier.

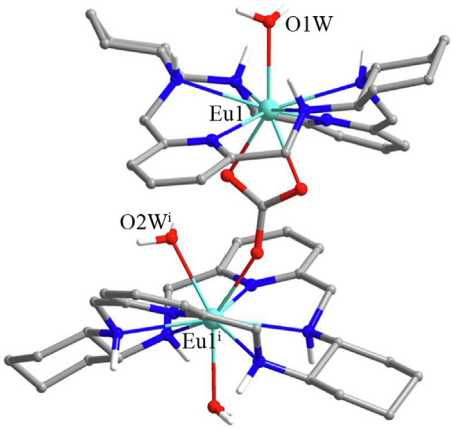

Fig. 15. Balls and sticks representation of the crystal structure of $[Eu_2(L^{15})_2(\mu_2\text{-}CO_3)(H_2O)_3]^{4+}$ in $[Eu_2(L^{15})_2(\mu_2\text{-}CO_3)(H_2O)_3]Cl_4$. Color codes: blue-green: dysprosium; blue: nitrogen; red: oxygen; gray: carbon; white: hydrogen. Symmetry code ^{i} $-x+1$, $-y+1$, z. Reproduced with permission from Ref. 36. Copyright 2019 Elsevier.

4.1. Chirality

The introduction of chirality in lanthanoid complexes is a field of growing interest due to the potential applications of these compounds. Thus, they have been successfully used as catalysts in enantioselective transformations,[43] and they are very promising as polarized luminescence emitters (CPL).[44] These latter ones are of great relevance as OLEDs, probes in bioassays, or even in optical information storage. Accordingly, although studies on chirality of lanthanoid complexes with macrocyclic ligands from 2015 onwards are limited, they deserve to be mentioned.

Some enantiomeric pure chiral Schiff base complexes were obtained by templating the carbonyl reactant with an enantiomeric pure amine in the presence of the lanthanoid salt. Thus, pure mononuclear enantiomeric complexes of the isomer L^{4RRRR} with Nd^{III} or Yb^{III} (Fig. 16),[20,21] L^{5RRRR} or L^{5SSSS} with Dy^{III},[22,23] L^{6RRRR} with La^{III} or Tb^{III},[24] and L^{7RRRR} or L^{7SSSS} with Dy^{III},[26] were reported. These chiral complexes seem stable in solution, retaining its chirality, while achiral $[Nd(L^{4SSRR})Cl(H_2O)_2]Cl_2$ converts to the racemic diastereomeric mixture of $[Nd(L^{4RRRR})Cl(H_2O)_2]Cl_2$ and $[Nd(L^{4SSSS})Cl(H_2O)_2]Cl_2$ over time.[20]

Reaction of the enantiomeric complexes with NaOH leads to dinuclear compounds that maintain their chirality,[21,35] and even racemic $[Yb_2(L^{4RRRR})_2(\mu\text{-}OH)_2(H_2O)_2][Yb_2(L^{4SSSS})_2(\mu\text{-}OH)_2(H_2O)_2](NO_3)_8$ (Fig. 17)[21] is obtained by mixing the corresponding enantiomeric *RRRR* or *SSSS* mononuclear complexes with the base, which confirms chiral recognition of macrocyclic units of the same chirality in solids. The same can be said for dinuclear enantiomeric *RRRR* fluoride bridged complexes of L^5 or L^6, which are isolated from the mononuclear enantiomers in the presence of an ionic fluoride.[24]

However, the chiral dinuclear complexes $[Dy_2(L^{5RRRR})_2(\mu\text{-}OH)_2(4\text{-}MeSPhO)_2](BPh_4)$ and $[Dy_2(L^{5SSSS})_2(\mu\text{-}OH)_2(4\text{-}MeSPhO)_2](BPh_4)$ are obtained in one pot template synthesis,[22] and not from the monomeric units, as stated above. In this case, the crystals are not only enantiomorphic but polar. Despite the polar character, ferroelectric behavior was not observed for none of the enantiomers.

In addition, a chiral mononuclear Dy^{III} complex of the amine L^{15RRRR},[36] and Yb^{III} and Eu^{III} complexes of the mixed imine-amine L^{17RR} and L^{17SS} donors,[38] were obtained from the free pure enantiomeric ligands. The chirality of the europium complex $[EuL^{17RR}(NO_3)_2](NO_3)$ is accompanied by luminescence, which indicates the ligand-to-metal energy transfer in this complex.[38]

It is also worth noting that the chirality of the species cannot reside in the N_6 or N_5 donor, but also in the auxiliary ligands. Thus, the pure enantiomers $[DyL^{14}(BINOL^{R})_2](BPh_4)$ or $[DyL^{14}(BINOL^{S})_2](BPh_4)$ (Fig. 18)[22] can be obtained from the pure *R* or *S* ancillary oxygen donor.

4.2. Biological activity

Some of the lanthanoid complexes with N_6 donors have shown some kind of biological activity. Thus, the dinuclear complex $[Eu_2(L^{15})_2(\mu_2\text{-}CO_3)(H_2O)^3]Cl_4$[36] shows considerable activity as a catalyst for the hydrolysis of bis(4-nitrophenyl)phosphate, with an observed rate $k_{obs} = 6.5 \times 10^{-5}$ s^{-1}. The activity of this carbonate bridged species is higher than that found for all the tested monomeric lanthanoid complexes with the L^{15} ligand. This likely results from cooperative action of the two Eu^{III} ions within the carbonate bridges.[36]

$[LaL^9(MeOH)(NO_3)_2](NO_3)$ interacts with DNA, being able to form complexes with "non-G4" Tel26.[28] This complex causes important conformational changes in the "non-G4" Tel26, as shown by circular dichroism, and it is hypothesized that it is an active agent binding probably by $\pi-\pi$-stacking and electrostatic interactions to the apex of the folded hybrid type G4 DNA, thus stabilizing it.

The complexes $[LaL^X(NO_3)_3]$ (X = 8 or 9),[45] with a supposed structure based on B3LYP calculations like that of $[LnL^1(NO_3)_3]$ (Ln = Ce, Pr)[16] or $[LnL^3(NO_3)_3]$ (Ln = La, Ce),[19] intercalate in DNA. $[LaL^8(NO_3)_3]$ shows more propensity to intercalate between DNA base pairs than $[LaL^9(NO_3)_3]$, due to the more twisted structure of

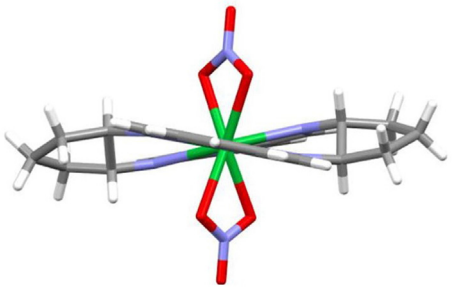

Fig. 16. Balls and sticks representation of the crystal structure of $[Yb(L^{4RRRR})(NO_3)_2]^{+}$ in $[Yb(L^{4RRRR})(NO_3)_2](NO_3)$. Color codes: green: ytterbium; blue: nitrogen; red: oxygen; gray: carbon; white: hydrogen. Reproduced with permission from Ref. 21. Copyright 2020 Elsevier.

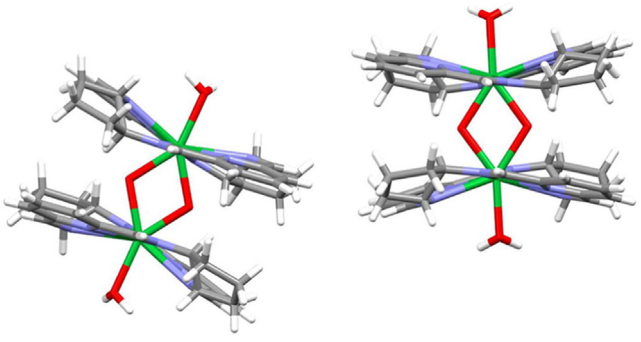

Fig. 17. Sticks diagrams for $[Yb_2(L^{4RRRR})_2(\mu\text{-}OH)_2(H_2O)_2]^{2+}$ and $[Yb_2(L^{4SSSS})_2(\mu\text{-}OH)_2(H_2O)_2]^{2+}$ cations in $[Yb_2(L^{4RRRR})_2(\mu\text{-}OH)_2(H_2O)_2][Yb_2(L^{4SSSS})_2(\mu\text{-}OH)_2(H_2O)_2](NO_3)_8$. Color codes: green: Yb; blue: N; red: O; gray: C; white: H. Reproduced with permission from Ref. 21. Copyright 2020 Elsevier.

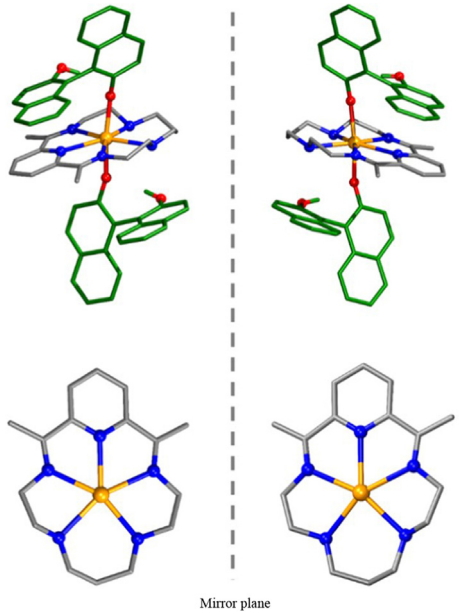

Fig. 18. Structure of the cation (top) and equatorial plane (bottom) in $[DyL^{14}(BINOL^{X})_2](BPh_4)$ ($X = R, S$). Reproduced with permission from Ref. 22. Copyright 2022 Chinese Chemical Society.

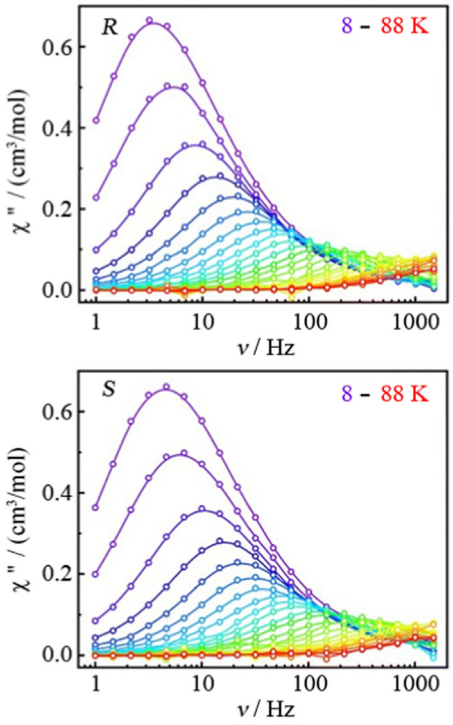

Fig. 19. Frequency dependence of the out-of-phase component of the ac susceptibility (χ'') at different temperatures for: up) $[Dy(L^{5RRRR})(Ph_3SiO)_2][(4\text{-Br-Ph})BPh_3]$; bottom) $[Dy(L^{5SSSS})(Ph_3SiO)_2][(4\text{-Br-Ph})BPh_3]$. Reproduced with permission from Ref. 23. Copyright 2022 Royal Society of Chemistry.

the latter complex. However, both compounds show photocleavage DNA activity, and $[LaL^8(NO_3)_3]$ presents more inhibitory *in vitro* activity against leukemia cancer cell line, in agreement with its higher ability for intercalation between the base pairs of the DNA. Nevertheless, the most hydrophobic complex $[LaL^9(NO_3)_3]$ shows greater affinity to join bovine serum albumin in water, which is relevant from the point of view that it can deliver in the body and penetrate to the cell easier.

4.3. Molecular magnetism

The magnetic properties of most of the reported mononuclear complexes with PBP and HBP geometry,[22–27,30–32] were recently summarized.[14] In addition to the compounds already listed in the article by Gil et al.,[14] there are 9 other mononuclear compounds with N_5 or N_6 macrocycles whose behavior as molecule magnets has not been reviewed until now.[23,31,32] The only complex with an N_5 donor for which there is no crystal structure but strong structural evidence of its PBP geometry, was published in 2014,[31] but it is included in this review because of its interest in comparison to properties.

Given that some magneto-structural aspects of the previously reviewed complexes have not been discussed, they are included in this revision, which will address the influence of different structural parameters on magnetic properties (Tables 4 and 5). From these tables it is apparent that:

1. The *R/S* isomerism does not seem to have great influence on the magnetic properties of the compounds, since the effective energy barriers for the reversal of the magnetization (U_{eff}) of both *R* and *S* isomeric complexes of L^5 (Fig. 19),[22,23] L^7(Table 4),[26] or BINOL[22] (Table 5) are equal if the standard deviations are considered.
2. Counterions also do not appear to have a strong influence on energy barriers, as previously stated by *ab initio* calculations.[27] Accordingly, if we compare the U_{eff} values between pairs $[DyL^{11}(Ph_3SiO)_2](ClO_4)$ and $[DyL^{11}(Ph_3SiO)_2](OTf)$, $[DyL^8(Ph_3SiO)_2](BPh_4)$ and $[DyL^8(Ph_3SiO)_2](PF_6)$, and among the six isomers $[Dy(L^{5XXXXX})(Ph_3SiO)_2](BPh_4)$, $[Dy(L^{5XXXX})(Ph_3SiO)_2][(3\text{-Br-Ph})BPh_3]$ or $[Dy(L^{5XXXX})(Ph_3SiO)_2][(4\text{-Br-Ph})BPh_3]$ (X = *R* or *S*), the energy barriers do not differ significantly.
3. The U_{eff} value does not depend on a single structural factor (Tables 4 and 5). Thus, there appear to be many factors that exert a strong influence on the energetics as a whole, but not individually. In this way, the following aspects should be taken into account:

   3.1. The deviation from the ideal geometry: the smallest deviations (ChSM values)[41] occur in the derivatives of L^6, L^7 and L^{11}. However, the compounds with the least distorted geometry are those of L^6, but these are not the ones that reach the highest barriers. In turn, these complexes also show the least deviation of the N-donors from the calculated equatorial N_6 plane (Table 4), with the Dy atom protruding less from this plane. Thus, a less distorted geometry does not necessarily mean a higher barrier, contrary to what was previously suggested.[14]

   3.2. The increase in the O—Dy—O angle is not directly proportional to an increase in the energy barrier. Therefore, compounds with an ideal angle of 180° (as $[DyL^6(PhO)_2](BPh_4)$ and $[DyL^6(4\text{-MeO-PhO})_2](BPh_4)$, Table 4) do not have the highest energy barrier. Even $[DyL^6(naphtolate)_2](BPh_4)$, with an O—Dy—O angle of 168.9(2)°, among the smallest for this group of compounds, shows higher U_{eff} than compounds with much larger angles, such as those derived from L^8 (angles as open as 179.8(3)°).

   3.3. The shorter Dy—O apical distance by itself does not imply a higher energy barrier. This is perfectly demonstrated by the L^6 derivatives, which show the shortest Dy—O distances but not the highest U_{eff}.

Table 4
Some structural and magnetic parameters for mononuclear Dy^{III} complexes with N_6 macrocycles and HBP geometry (c.n. = 8) studied as molecule magnets.

Metal complex[a]	ChSM[b]	Dy–N ($\times 10^{-1}$ nm)	Dy–O ($\times 10^{-1}$ nm)	Dev. N-plane ($\times 10^{-1}$ nm)[c]	Dev. Dy-plane ($\times 10^{-1}$ nm)[d]	α (O–Dy–O) (°)	θ (planes)[e] (°)	Plane subst.[f]	U_{eff} (K)[g]	T_b (K) hysteresis[h]	Ref.
[Dy(L^{5RRRR})($Ph_3SiO)_2$](BPh_4)	1.933	2.616(4) −2.712(3)	2.123(3) 2.139(3)	0.113–0.440	0.095	178.1(1)	87.87	ED	1455	5 (3.1)	22
[Dy(L^{5SSSS})($Ph_3SiO)_2$](BPh_4)	1.904	2.618(5) −2.710(4)	2.128(4) 2.141(3)	0.110–0.437	0.096	178.5(1)	87.74	ED	1457	5 (3.1)	22
[Dy(L^{5RRRR})($Ph_3SiO)_2$] [(3-Br-Ph)BPh_3]	1.977	2.608(5) −2.720(5)	2.131(4) 2.138(4)	0.096–0.442	0.094	175.5(2)	87.46	ED	1363	4 (4)	23
[Dy(L^{5SSSS})($Ph_3SiO)_2$] [(3-Br-Ph)BPh_3]	1.964	2.597(7) −2.718(6)	2.133(5) 2.137(5)	0.095–0.441	0.092	175.0(2)	87.41	ED	1415	1.9 (4)	23
[Dy(L^{5RRRR})($Ph_3SiO)_2$] [(4-Br-Ph)BPh_3]	1.897	2.618(9) −2.699(8)	2.136(7) 2.145(7)	0.116–0.441	0.101	178.4(3)	88.21	ED	1369	1.9 (4)	23
[Dy(L^{5SSSS})($Ph_3SiO)_2$] [(4-Br-Ph)BPh_3]	1.909	2.623(7) −2.702(7)	2.140(6) 2.141(5)	0.116–0.435	0.105	179.1(2)	88.43	ED	1434	1.9 (4)	23
[DyL^6($PhO)_2$](BPh_4)	1.069	2.669(5) −2.689(6)	2.108(6)	0.022	0	180	90	EW	1100	2 (1.2)	25
[DyL^6(4-MeO-$PhO)_2$](BPh_4)	1.028	2.678(5) −2.704(6)	2.089(6)	0.03	0	180	90	EW	1338	6 (1.2)	25
[DyL^6(naphtholate)$_2$](BPh_4)	1.249	2.653(6) −2.737(7)	2.084(6) 2.100(6)	0.010–0.042	0.003	168.9(2)	89.23	EW	1226	6 (1.2)	25
[DyL^{7RRRR}($Ph_3SiO)_2$](PF_6)	1.338	2.675(8) −2.744(7)	2.124(6) 2.139(7)	0.014–0.228	0.022	177.9(2)	85.66	EW	1833	n.r.	26
[DyL^{7SSSS}($Ph_3SiO)_2$](PF_6)	1.332	2.664(7) −2.736(5)	2.122(6) 2.147(6)	0.007–0.221	0	178.8(2)	85.56	EW	1819	20 (20)	26
[DyL^8(2,4-di-^{t}Bu-$PhO)_2$](BPh_4)	2.472	2.5722(17) −2.6383(17)	2.1303(14) 2.1456(14)	0.088–0.540	0.073	173.56(6)	86.89	ED	973	3 (4)	27
[DyL^8($Ph_3SiO)_2$](BPh_4)	2.163	2.6057(18) −2.635(2)	2.1425(16) 2.1514(16)	0.195–0.518	0.024	176.14(7)	88.15	ED	1124	5 (4)	27
[DyL^8($Ph_3SiO)_2$](PF_6)	2.271	2.551(6) −2.642(6)	2.153(7) 2.163(6)	0.076–0.530	0.074	179.8(3)	84.41	ED	1080	n.r.	27
[DyL^{11}($Ph_3SiO)_2$](ClO_4)	1.347	2.642(3) −2.695(3)	2.138(2) 2.141(2)	0.082–0.296	0.002	175.53(9)	86.21	EW	1732	10 (4)	23
[DyL^{11}($Ph_3SiO)_2$](OTf)	1.281	2.646(4) −2.704(4)	2.129(4) 2.142(2)	0.100–0.287	0.003	177.1(2)	86.88	EW	1680	6 (4)	23

[a] Solvates are omitted; n.r.: not reported.
[b] According to SHAPE.
[c] Distance from the equatorial N-atoms to the mean calculated N_6 plane in nm.
[d] Distance from the Dy^{III} ion to the mean calculated N_6 plane in nm.
[e] Angle between equatorial N_6 and axial O–Dy–O planes.
[f] Character of the substituents of the imine moieties: ED: electron-donating, EW: electron-withdrawing.
[g] $H_{dc} = 0$
[h] In parentheses sweep rate in mT/s.

3.4. The angle between the equatorial N_5 or N_6 plane and the O–Dy–O axial plane (Tables 4 and 5) does not seem to have any direct correlation with the energy barrier, since small angles can lead to large barriers, and *vice versa.*

3.5. The introduction of electron-donating substituents in the RO^- apical donors seems to have a profound impact on U_{eff}, as expected. Accordingly, the energy barrier of [DyL^6(4-MeO-$PhO)_2$](BPh_4) (1338 K) is significantly higher than that of [DyL^6($PhO)_2$](BPh_4) (1100 K), in spite of the very similar structural parameters. Following this pattern, electron-withdrawing substituents on the axial ligands produces a very noticeable lowering of the energy barrier, as exemplified by [DyL^{14}(2,6-Cl,4-NO_2-$PhO)_2$](BPh_4) (Table 5), which, surprisingly, shows no single ion magnet behavior in the absence of an external applied magnetic field (Table 5), in spite of the apparently highly axial PBP geometry.

3.6. The introduction of electron-withdrawing substituents on the macrocycle ligand also seems to greatly influence U_{eff}, and the blocking temperatures. Accordingly, if we compare complexes with the same apical donors, i.e., the most abundant group with triphenylsilanolate axial ligands (Tables 4 and 5, 14 complexes), the highest U_{eff} and T_b values are achieved by compounds with the L^7 macrocycle, with 2,4-F-Ph substituents. This agrees with a weaker equatorial field, shown by the longest Dy–N distances among this group. In addition, these withdrawing substituents also seem to disfavor the quantum channel of the magnetization (QTM) in compounds with N_6 donors, given that only for [DyL^{7RRRR}($Ph_3SiO)_2$](PF_6) and [DyL^{7SSSS}($Ph_3SiO)_2$](PF_6) this mechanism does not seem to be operative. This absence of QTM supposes a great increase in the blocking temperature, which is maximum (20 K) for [DyL^{7SSSS}($Ph_3SiO)_2$](PF_6) (Fig. 20)[26] among this kind of compound.

For the other complexes with N_6 macrocycles (Table 4), the magnetic hysteresis loops show butterfly shapes, which confirm the presence of QTM processes at low temperatures,[22,23,25,27] as exemplified in Fig. 21 for [DyL^8($Ph_3SiO)_2$](BPh_4).

3.7. A weaker equatorial field by itself does not suppose a higher energy barrier, given that de Dy–N distances for [DyL^{7SSSS}($Ph_3SiO)_2$](PF_6) and [DyL^6(naphtholate)$_2$](BPh_4) are very similar, but U_{eff} is significantly lower for the latter complex.

3.8. The delocalization of charge in the equatorial plane also seems to increase the energy barrier. In this way, the complexes [DyL^{11}($Ph_3SiO)_2$](ClO_4) and [DyL^{11}($Ph_3SiO)_2$](OTf) are

Table 5
Some structural and magnetic parameters for mononuclear Dy^{III} complexes with N_5 macrocycles and PBP geometry (c.n. = 7) studied as molecule magnets.

Metal complex[a]	ChSM[c]	Dy–N ($\times10^{-1}$ nm)	Dy–O ($\times10^{-1}$ nm)	Dev. N-plane[d] ($\times10^{-1}$ nm)	Dev. Dy-plane[e] ($\times10^{-1}$ nm)	α (O–Dy–O) (°)	θ (planes)[f] (°)	Plane subst.[g]	U_{eff}[h] (K)	T_b (K) hysteresis[j]	Ref.
$[DyL^{12}(Ph_3SiO)_2](BPh_4)$	A: 1.295 B: 1.681	A: 2.400(5) −2.570(5) B: 2.457(5) − 2.564(5)	A 2.136(4) 2.157(3) B: 2.158(4) 2.161 (4)	A: 0.053–0.197 B: 0.025–0.328	A: 0.058 B: 0.113	A: 176.5(2) 173.1(2)	87.08 89.20	ED	1108	14 (10)	30
$[DyL^{13}(Cl)_2](Cl)$[b]									23.7, 4.1	n.r.	31
$[DyL^{14}(BINOL^R)_2](BPh_4)$	1.680	2.425(6) −2.488(7)	2.150(5) 2.184(5)	0.021–0.118	0.134	166.9(2)	84.79	ED	403	<1.9 (3.1)	22
$[DyL^{14}(BINOL^S)_2](BPh_4)$	1.690	2.416(9) −2.486(10)	2.149(8) 2.177(7)	0.020–0.114	0.134	167.3(3)	85.16	ED	404	<1.9 (3.1)	22
$[DyL^{14}Ph_3SiO)_2](BPh_4)$	A: 1.241 B: 1.390	A: 2.426(5) −2.484(6) B: 2.429(7) −2.496(6)	A: 2.150(4) 2.173(4) B: 2.157(4) 2.159(4)	A: 0.09–0.075 B: 0.012–0.081	A: 0.056 B: 0.081	A: 173.33(16) B: 170.78(16)	A: 89.32 B: 89.10	ED	1085	9 (20)	32
$[DyL^{14}(2,6\text{-}Cl,4\text{-}NO_2\text{-}PhO)_2](BPh_4)$	A: 1.235 B: 1.071	A: 2.406(8) −2.461(8) B: 2.361(7) −2.457(9)	A: 2.178(5) 2.207(5) B: 2.186(8) 2.189(7)	A: 0.003–0.024 B: 0.03–0.067	A: 0.076 B: 0.084	A: 168.5(2) B: 172.8(3)	A: 87.59 B: 89.88	ED	No signal 39[i]	<2.0 2.0[k]	32

[a] Solvates are omitted.
[b] Without crystal structure; n.r.: not reported.
[c] According to SHAPE.
[d] Distance from the equatorial N-atoms to the mean calculated N_6 plane.
[e] Distance from the Dy^{III} ion to the mean calculated N_6 plane.
[f] Angle between equatorial N_5 and axial O–Dy–O planes.
[g] Character of the substituents of the imine moieties: ED: electron-donating.
[h] $H_{dc} = 0$.
[i] U_{eff} value under a dc field of 0.02 T.
[j] In parentheses sweep rate in mT/s.
[k] Diluted sample.

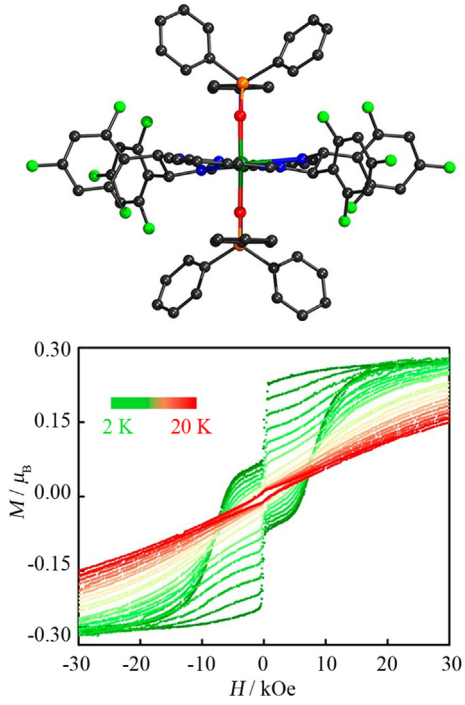

Fig. 20. Up) Ellipsoids diagram for the cation $[DyL^{7RRRR}(Ph_3SiO)_2]^+$ in $[DyL^{7RRRR}(Ph_3SiO)_2](PF_6)$. Color codes: deep green: dysprosium; blue: nitrogen; red: oxygen; gray: carbon; light green: fluoride. Hydrogen atoms are omitted. Bottom) Hysteresis graph, showing T_B = 20 K. Adapted with permission from Ref. 26. Copyright 2021 American Chemical Society.

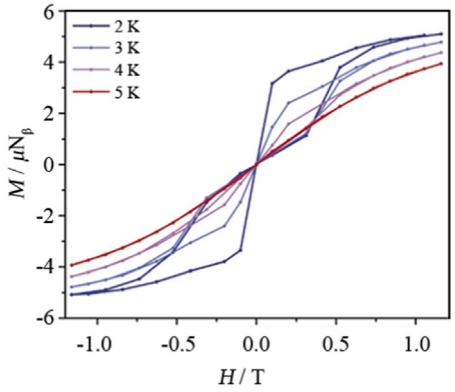

Fig. 21. Butterfly-like hysteresis loops for $[DyL^8(Ph_3SiO)_2](BPh_4)$. Adapted with permission from Ref. 27. Copyright 2019 Wiley.

the second in values of U_{eff} and T_b (Fig. 22, Table 4) among those with N_6 macrocycles. Obviously, this delocalization should give rise to a nearly perfect equatorial N_6 plane, but this plane is less distorted in complexes of the apparently more flexible ligand L^6, which show lower energy barriers. Accordingly, although a single example is not sufficient to establish a trend, the complexes of L^{11} reinforce the idea that the planarity of the equatorial belt does not seem to be an indicator of higher energy barriers by itself, and suggest that π delocalization in the equatorial plane appears to play an important role in U_{eff}.

3.9. The scarce number of complexes with PBP geometry (Table 5) prevents major conclusions, but it is still possible to perceive that:

3.9.1. Small differences in the length of the carbon chain between N-donors of the macrocycle ligand does not introduce

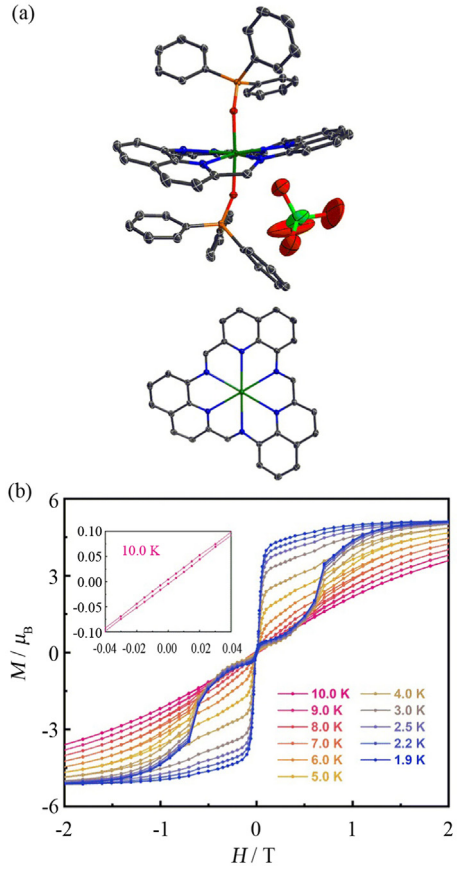

Fig. 22. (a) Ellipsoids diagram for the $[DyL^{11}(Ph_3SiO)_2](ClO_4)$. Color codes: deep green: dysprosium; blue: nitrogen; red: oxygen; gray: carbon; light green: chloride. (b) Hysteresis graph, showing T_B = 10 K. Hydrogen atoms are omitted. Adapted with permission from Ref. 23. Copyright 2022 Royal Society of Chemistry.

significant structural changes that affect the energy barrier, given that U_{eff} is equal for $[DyL^{12}(Ph_3SiO)_2](BPh_4)$ and $[DyL^{14}(Ph_3SiO)_2](BPh_4)$.

3.9.2. PBP entails a stronger equatorial field than HBP geometry, as it can be seen by the Dy—N distances. This stronger field does not seem to be due to the presence of electron-donating substituents in both L^{12} and L^{14} macrocycles, because the Dy—N distances in these PBP complexes are shorter than in those derived from L^8, which also has methyl groups attached to the imine moieties. In addition, this stronger field does not appear to disfavor the energy barrier, given that U_{eff} values in the PBP complexes $[DyL^{12}(Ph_3SiO)_2](BPh_4)$ and $[DyL^{14}(Ph_3SiO)_2](BPh_4)$ are similar to those of the HBP compounds $[DyL^8(Ph_3SiO)_2](BPh_4)$ and $[DyL^8(Ph_3SiO)_2](PF_6)$.

3.9.3. In spite of the similar energy barriers, T_b is apparently higher for the PBP complexes $[DyL^{12}(Ph_3SiO)_2](BPh_4)$ (Fig. 23)[30] and $[DyL^{14}(Ph_3SiO)_2](BPh_4)$ than for the HBP compounds $[DyL^8(Ph_3SiO)_2](BPh_4)$ and $[DyL^8(Ph_3SiO)_2](PF_6)$. However, these results should be taken with caution, since the measurement of the hysteresis cycles has been performed at lower sweep rate for the L^8 complexes. Therefore, more experiments with similar compounds with PBP and HBP geometry, whose magnetic properties have been studied under the same conditions, are needed to really establish a correlation.

3.9.4. The comparison of the L^{14} derivatives among them and with $[DyL^{12}(Ph_3SiO)_2](BPh_4)$ (Table 5) clearly shows the brutal impact of apical donors on energy barriers. Thus, $[DyL^{14}(BINOL^X)_2](BPh_4)$ (X = R or S) are the complexes with the most distorted geometry and the narrowest O—Dy—O angles, but they are not the ones with the lowest energy barrier, which is achieved by $[DyL^{14}(2,6\text{-Cl},4\text{-}NO_2\text{-PhO})_2](BPh_4)$. This indicates that the structural parameters alone cannot predict an increase in the energy barriers in Dy^{III} PBP or HBP complexes with a quite strong axial field, and that the electronic characteristics of the ligands are fundamental factors to take into account. Thus, the lower U_{eff} value of *ca.* 400 K for $[DyL^{14}(BINOL^X)_2](BPh_4)$ (X = R or S) compared with $[DyL^{12}(Ph_3SiO)_2](BPh_4)$ or $[DyL^{12}(Ph_3SiO)_2](BPh_4)$ (U_{eff} *ca.* 1100 K) cannot be justified by the small O—Dy—O angle of *ca.* 167°, as previously suggested[14] (U_{eff} for $[DyL^6(naphtholate)_2](BPh_4)$, with an O—Dy—O angle of 168.9(2)° is 1226 K), and the feasible lower Lewis base character of the binolate with respect to the triphenylsilanolate anion, probably derived from the higher conjugation of the former auxiliary ligand, should not be underestimated. This is also supported by the fact that the 2,6-Cl,4-NO_2-PhO^- axial ligand, with 3 electron-withdrawing substituents in the aromatic ring, and, therefore, an impoverished Lewis base character, prevents the compound $[DyL^{14}(2,6\text{-Cl},4\text{-}NO_2\text{-PhO})_2](BPh_4)$ from behaving as a molecule magnet.

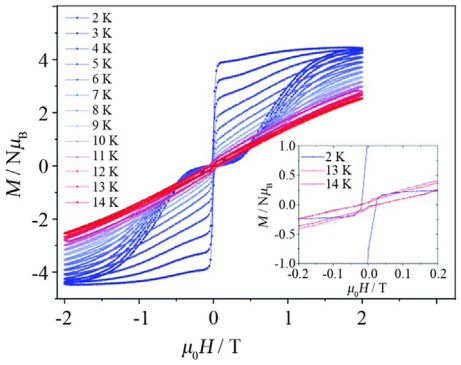

Fig. 23. Hysteresis loops for $[DyL^{12}(Ph_3SiO)_2](BPh_4)$. Reproduced with permission from Ref. 30. Copyright 2020 Royal Society of Chemistry.

Accordingly, the comparison of the complexes taking only into account the apical donors allows inferring that the best results are obtained with triphenylsilanolate, a ligand where the charge on the oxygen atom is not delocalized. Therefore, these results indicate that the possibility of π delocalization of the charge affecting the alcohol oxygen atom of the apical donor disfavors the barrier.

The following best results are obtained with the auxiliary ligand 4-MeO-PhO^-, which has a electron-donating group attached to the phenol ring, and this comparison also shows that naphtholate is a better donor than binolate, given the shorter Dy—O distances in $[DyL^6(naphtholate)_2](BPh_4)$ respect to $[DyL^{14}(BINOL^X)_2](BPh_4)$ (X = R or S). This is maybe a consequence of the more delocalization of the charge in the BINOL ligand. Furthermore, the comparison of the SIMs with N_5 donors (Table 5) corroborates, once again, that the monoatomic oxygen donors induce a stronger axial field than the chloride one.[30]

As a summary of all the aspects considered above, it seems that the key to obtain compounds with higher energy barriers using this kind of N_5 and N_6 ligands is the introduction of electron-withdrawing substituents in the macrocycles, which if possible should have high charge delocalization, and the use of axial O-

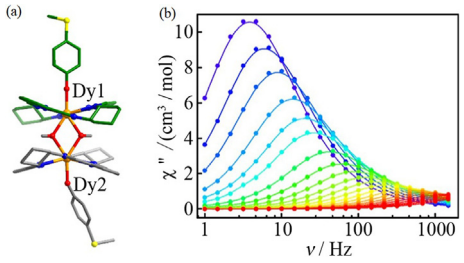

Fig. 24. (a) Ball and sticks diagram for the cation $[Dy_2(L^{5RRRR})_2(\mu\text{-}OH)_2(4\text{-}MeSPhO)_2]^+$ in $[Dy_2(L^{5RRRR})_2(\mu\text{-}OH)_2(4\text{-}MeSPhO)_2](BPh_4)$. Color codes: orange: dysprosium; blue: nitrogen; red: oxygen; green or gray: carbon; yellow: sulfur. (b) χ'' vs frequency at different temperatures. Hydrogen atoms are omitted. Adapted with permission from Ref. 22. Copyright 2022 Chinese Chemical Society.

donors with electron-donating substituents, and in which the charge on the oxygen atom is not delocalized.

Finally, the molecule magnet-like behavior of two dinuclear isomers derived from L^5, $[Dy_2(L^{5XXXX})_2(\mu\text{-}OH)_2(4\text{-}MeSPhO)_2](BPh_4)$ (X = *R* or *S*), is also described (Fig. 24).[22] The dysprosium atoms in these isomers are nonacoordinate, in hula-hoop environments, as shown in Table 2. These compounds are also SMMs at zero-field, but with much lower energy barriers, of *ca*. 150 K. Thus, it seems that, despite the ferromagnetic character of the magnetic coupling promoted by the OH^- bridge, it cannot compensate the weakening of the axial crystal field, and Raman relaxation is predominant in these SMMs.[22] Accordingly, once more, the best magnetic results are achieved by mononuclear complexes, where the anisotropy is easier to control.

5. Conclusions

This review summarizes the synthesis, characterization, and properties of lanthanoid complexes prepared from a family of N_5 and N_6 macrocycles from 2015 to date. It emphasizes the different methods of obtaining and, above all, of crystallizing these compounds, a task that is often arduous. This type of compound presents very varied properties, and thus it is easy to obtain enantiomeric pure chiral products simply starting from a pure enantiomeric amine. Some of these compounds have also demonstrated biological activity, with the cytostatic activity of several of the lanthanum complexes standing out. Magnetic studies of dysprosium complexes with these macrocycles, which are stable in air, have increased notably in the last 3 years. Most of these studies have been carried out on compounds with hexaaza macrocycles and HBP geometry, where the N_6 donor forms the equatorial plane. These studies show a quite good behavior of these complexes as molecule magnets. From them, it is inferred that the higher value of U_{eff} does not depend on a single structural factor, and that many factors exert a strong influence on the energy barrier as a whole, but not individually. Thus, the smaller deviation from the ideal geometry, the larger O—Dy—O angle, or the smaller Dy—O apical distance individually do not guarantee an increase in U_{eff}. In fact, the highest barriers, regardless of the macrocycle that fills the equatorial plane, are obtained with triphenylsilanolate as the axial ligand, the only O-donor where there is no delocalization of the charge on the oxygen atom. Besides, the introduction of electron-donating substituents in phenolate ancillary axial donors also increase U_{eff}, while electron-withdrawing groups lower this barrier. Nevertheless, the presence of electron-withdrawing substituents on the N_6 macrocycle enhances U_{eff} and diminishes the QTM effect, improving the blocking temperature, with a record of 20 K for this kind of complex. Accordingly, the electronic characteristics of the ligands themselves seem to be of greater importance in the energy barrier for the reversal of the magnetization than an ideal geometry.

Declaration of competing interest

The authors declare that they have no conflict of interest.

Acknowledgments

J.C-V acknowledges Xunta de Galicia for his postdoctoral fellowship (ED481B-2022-068). P.O-M. thanks the Fundación Segundo Gil Dávila for her PhD fellowship.

Appendix A. Supplementary data

Supplementary data to this article can be found online at https://doi.org/10.1016/j.jre.2023.03.013.

References

1. Bernot K, Daiguebonne C, Calvez G, Suffren Y, Guillou O. A journey in lanthanide coordination chemistry: from evaporable dimers to magnetic materials and luminescent devices. *Acc Chem Res*. 2021;54(2):427.
2. Zabala-Lekuona A, Seco JM, Colacio E. Single-molecule magnets: from Mn12-ac to dysprosium metallocenes, a travel in time. *Coord Chem Rev*. 2021:441.
3. Pellissier H. Recent developments in enantioselective lanthanide-catalyzed transformations. *Coord Chem Rev*. 2017;336:96.
4. Rocha J, Brites CDS, Carlos LD. Lanthanide organic framework luminescent thermometers. *Chem Eur J*. 2016;22(42):14782.
5. Wahsner J, Gale EM, Rodríguez-Rodríguez A, Caravan P. Chemistry of MRI contrast agents: current challenges and new frontiers. *Chem Rev*. 2019;119(2):957.
6. Rezaeivala M, Keypour H. Schiff base and non-Schiff base macrocyclic ligands and complexes incorporating the pyridine moiety – the first 50 years. *Coord Chem Rev*. 2014;280:203.
7. Gavey EL, Pilkington M. Coordination complexes of 15-membered pentadentate aza, oxoaza and thiaaza Schiff base macrocycles "Old Complexes Offer New Attractions". *Coord Chem Rev*. 2015;296:125.
8. Benelli C, Gatteschi D. *Introduction to molecular magnetism: from transition metals to lanthanides*. Hoboken: Wiley; 2015.
9. Meng YS, Jiang SD, Wang BW, Gao S. Understanding the magnetic anisotropy toward single-ion magnets. *Acc Chem Res*. 2016;49(11):2381.
10. Rinehart JD, Long JR. Exploiting single-ion anisotropy in the design of f-element single-molecule magnets. *Chem Sci*. 2011;2(11):2078.
11. Guo FS, Day BM, Chen YC, Tong ML, Mansikkam-ki A, Layfield RA. Magnetic hysteresis up to 80 kelvin in a dysprosium metallocene single-molecule magnet. *Science*. 2018;362:1400.
12. Ashebr TG, Li H, Ying X, Li XL, Zhao C, Liu S, et al. Emerging trends on designing high-performance dysprosium(III) single-molecule magnets. *ACS Mater Lett*. 2022;4:307.
13. Groom CR, Bruno IJ, Lightfoot MP, Ward SC. The Cambridge structural database. *Acta Crystallogr, Sect B: Struct Sci, Cryst Eng Mater*. 2016;72(2):171.
14. Gil Y, Castro-Alvarez A, Fuentealba P, Spodine E, Aravena D. Lanthanide SMMs based on belt macrocycles: recent advances and general trends. *Chem Eur J*. 2022;28:e202200336.
15. Gil Y, Fuentealba P, Vega A, Spodine E, Aravena D. Control of magnetic anisotropy by macrocyclic ligand distortion in a family of Dy^{III} and Er^{III} single molecule magnets. *Dalton Trans*. 2020;49(48):17709.
16. Starynowicz P, Lisowski J. Monomeric, dimeric and polymeric lanthanide(III) complexes of a hexaazamacrocyclic imine derived from 2,6-diformylpyridine and ethylenediamine. *Polyhedron*. 2015;85:232.
17. Villagra D, Fuentealba P, Spodine E, Vega A, Costa de Santana R, Verdejo R, et al. Effect of terbium(III) species on the structure and physical properties of polyurethane (TPU). *Polymer*. 2021;233:124209.
18. Fuentealba P, Villagra D, Gil Y, Aguilar-Bolados H, Costa de Santana R, Gasparotto G, et al. Thermal dependence of the luminescent properties of mononuclear TbIII macrocyclic complexes. *Eur J Inorg Chem*. 2021:4543.
19. Gajarushi AS, Wasim M, Nabi R, Kancharlapalli S, Rao VR, Rajaraman G, et al. Lanthanide complexes as molecular dopants for realizing air-stable n-type graphene logic inverters with symmetric transconductance. *Mater Horiz*. 2019;6(4):743.
20. Gregoliński J, Ślepokura K. Lanthanide(III) and yttrium(III) coordination compounds of diastereomeric (2+2) macrocyclic imines derived from 2,6-diformylpyridine and trans-1,2-diaminocyclopentane. *Polyhedron*. 2018;147:15.
21. Gregoliński J, Ślepokura K. Monomeric and dimeric nitrate lanthanide(III) and yttrium(III) coordination compounds of (2 + 2) imine macrocycle derived from 2,6-diformylpyridine and trans-1,2-diaminocyclopentane. *Polyhedron*. 2020;181:114433.

22. Zhu Z, Zhao C, Zhou Q, Liu S, Li XL, Mansikkamäki A, et al. Air-stable Dy(III)-macrocycle enantiomers: from chiral to polar space group. *CCS Chem*. 2022;4:3762.
23. Liu S, Gil Y, Zhao C, Wu J, Zhu Z, Li XL, et al. A conjugated Schiff-base macrocycle weakens the transverse crystal field of air-stable dysprosium single-molecule magnets. *Inorg Chem Front*. 2022;9:4982.
24. Ślepokura K, Cabreros TA, Muller G, Lisowski J. Sorting phenomena and chirality transfer in fluoride-bridged macrocyclic rare earth complexes. *Inorg Chem*. 2021;60:18442.
25. Li ZH, Zhai YQ, Chen W-P, Ding YS, Zheng YZ. Air-stable hexagonal bipyramidal dysprosium(III) single-ion magnets with nearly perfect D_{6h} local symmetry. *Chem Eur J*. 2019;25:16219.
26. Zhu Z, Zhao C, Feng T, Liu X, Ying X, Li XL, et al. Air-stable chiral single-molecule magnets with record anisotropy barrier exceeding 1800 K. *J Am Chem Soc*. 2021;143:10077.
27. Canaj AB, Dey S, Martí ER, Wilson C, Rajaraman G, Murrie M. Insight into D_{6h} symmetry: targeting strong axiality in stable dysprosium(III) hexagonal bipyramidal single-ion magnets. *Angew Chem Int Ed*. 2019;58:14146.
28. Fik-Jaskółka MA, Pospieszna-Markiewicz I, Roviello GN, Kubicki M, Radecka-Paryzek W, Patroniak V. Synthesis and spectroscopic investigation of a hexaaza lanthanum(III) macrocycle with a hybrid-type G4 DNA stabilizing effect. *Inorg Chem*. 2021;60:2122.
29. Starynowicz P, Lisowski J. Chirality transfer between hexaazamacrocycles in heterodinuclear rare earth complexes. *Dalton Trans*. 2019;48:8717.
30. Canaj AB, Dey S, Wilson C, Céspedes O, Rajaraman G, Murrie M. Engineering macrocyclic high performance pentagonal bipyramidal Dy(III) single-ion magnets. *Chem Commun*. 2020;56:12037.
31. Gavey EL, Beldjoudi Y, Rawson JM, Stamatatos TC, Pilkington M. Slow relaxation in the first penta-aza Dy(III) macrocyclic complex. *Chem Commun*. 2014;50:3741.
32. Zhang B, Guo X, Tan P, Lv W, Bai X, Zhou Y, et al. Axial ligand as a critical factor for high-performance pentagonal bipyramidal Dy(III) single-ion magnets. *Inorg Chem*. 2022;61:19726.
33. Tan P, Yang Y, Lv W, Jing R, Cui H, Zheng SJ, et al. A cyanometallate- and carbonate-bridged dysprosium chain complex with a pentadentate macrocyclic ligand: synthesis, structure, and magnetism. *New J Chem*. 2022;46:7892.
34. Fenton DE, Vigato PA. Macrocyclic Schiff base complexes of lanthanides and actinides. *Chem Soc Rev*. 1988;17:69.
35. Benetollo F, Bombieri G, Fonda KK, Polo A, Quagliano JR, Vallarino LM. Complexes of the lanthanide(III) ions with an aromatic six-nitrogen-donor macrocyclic ligand. *Inorg Chem*. 1991;30:1345.
36. Gerus A, Ślepokura K, Lisowski J. Carbonate-bridged dinuclear lanthanide(III) complexes of chiral macrocycle. *Polyhedron*. 2019;170:115.
37. Lamelas R, Bastida R, Labisbal E, Macías A, Pereira T, Pérez-Lourido P, et al. A new series of lanthanide complexes with the trans-disubstituted Py_2[18]aneN_6 macrocyclic ligand: synthesis, structures and properties. *Polyhedron*. 2019;160:180.
38. Wolska K, Janczak J, Gawryszewska P, Lisowski J. Rare earth complexes of chiral unsymmetrical hexaazamacrocycles. *Polyhedron*. 2021;198:115057.
39. Fitzsimmons PM, Jackels SC. Helical hexaazamacrocyclic ligands containing pyridyl and (+ or −)-*trans*-diaminocyclohexyl groups: effect of ligand constraints upon metal ion binding. *Inorg Chim Acta*. 1996;246:301.
40. Lamelas R, Garcia V, Linares A, Bastida R, Labisbal E, Fernandez-Lodeiro A, et al. Novel trans-disubstituted hexaaza-macrocyclic ligands containing pyridine head units: synthesis, disubstitution and colorimetric properties. *Sens. Actuators B Chem*. 2016;225:481.
41. Ruiz-Martínez A, Casanova D, Alvarez S. Polyhedral structures with an odd number of vertices: nine-coordinate metal compounds. *Chem Eur J*. 2008;14:1291.
42. Llunell M, Casanova D, Cirera J, Alemany P, Alvarez S. *SHAPE: Program for the stereochemical analysis of molecular fragments by means of continuous shape measures and associated tools*. Spain: University of Barcelona; 2010.
43. Pellissier H. Recent developments in enantioselective lanthanide-catalyzed transformations. *Coord Chem Rev*. 2017;336:96.
44. Wong HY, Lo WS, Yim KH, Law GL. Chirality and chiroptics of lanthanide molecular and supramolecular assemblies. *Chem*. 2019;5:3058.
45. Asadi Z, Mosallaei H, Sedaghat M, Yousefi R. Competitive binding affinity of two lanthanum(III) macrocycle complexes toward DNA and bovine serum albumin in water. *J Iran Chem Soc*. 2017;14:2367.